https://doi.org/10.5194/gmd-2021-34
Preprint. Discussion started: 29 March 2021

Geoscientific Model Development
Discussions
Open Access

An automatic lake-model application using near real-time data forcing: Development of an operational forecast model for Lake Erie

Shuqi Lin[1], Leon Boegman[1], Shiliang Shan[2], Ryan Mulligan[1]

[1]Department of Civil Engineering, Queen's University, Kingston ON Canada K7L 3N6
[2]Department of Physics and Space Science, Royal Military College of Canada, Kingston ON Canada K7K 7B4.
Correspondence to: Shuqi Lin (shuqi.lin@queensu.ca)

Abstract. For enhanced public safety and water resource management, a three-dimensional operational lake hydrodynamic forecast system called COASTLINES (Canadian cOASTal and Lake forecastINg modEl System) was developed. The modelling system is built upon the Aquatic Ecosystem Model (AEM3D) model, with predictive simulation capabilities developed and tested for a large lake (i.e., Lake Erie). The open-access web-based platform derives model forcing, code execution, post-processing and visualization of the model outputs, including water level elevations and temperature, is in near real-time. COASTLINES currently generates 240-h predictions using atmospheric forcing from 15 km and 25 km horizontal-resolution operational meteorological products from the Environment Canada Global Deterministic Forecast System (GDPS). Simulated water levels were validated against observations from 6 gauge stations, with model error increasing for longer forecast times. Satellite images and lake buoys were applied to validate forecast lake surface temperature (LST) and the water column thermal stratification. The forecast LST is as accurate as hindcasts, with a root-mean-square-deviation <2°C. COASTLINES predicts storm-surge events and up-/down-welling events that are important for flood water and drinking water/fishery management, respectively. Model forecasts are available in real-time at https://coastlines.engineering.queensu.ca/. This study provides an example of the successful development of an operational forecasting system, entirely driven by open-access data, that may be easily adapted to simulate aquatic systems or to drive other computational models, as required for management and public safety.

1 Introduction

Lakes hold a large proportion of the global surface freshwater, which supports biodiversity and supplies water resources for drinking, transportation and recreation. However, anthropogenic stressors are causing significant changes in the properties of lakes, such as rapid warming of surface water (O'Reilly et al., 2015), major seasonal water level fluctuations (Gronewold and Rood, 2019), increased frequency of extreme events (Saber et al., 2020) and severe water quality issues such as oxygen depletion (Rowe et al., 2019; Scavia et al., 2014) and harmful algal blooms (Brookes and Carey, 2011; Watson et al., 2016). Effort has been spent on investigating the long-term responses of physical processes in lakes to climate change (O'Reilly et al., 2015; Woolway and Merchant, 2019), but improving lake monitoring and developing short-term forecast models, to predict the occurrence of extreme events is also necessary (Woolway et al., 2020). The biogeochemical cycles in lakes are complex and often regulated by physical forcing; therefore, the first step to model and forecast water quality issues, like harmful algal blooms (Paerl et al., 2011; O'Neil et al., 2012) and hypoxia (Rao et al., 2008; Rao et al., 2014), is the development of accurate hydrodynamic hindcast and forecast models.

Over the past several decades, many computational fluid dynamics models have been applied to hindcast lake hydrodynamics to aid management. These range from one-dimensional (1D) models such as DYRESM (Antenucci and Imerito, 2000), Simstrat (Gaudard et al., 2017), and GLM (Hipsey et al., 2014), to three-dimensional (3D) models such as Delft3D (Lesser et al., 2004), FVCOM (Chen et al., 2013; Gronewold et al., 2019; Rowe et al., 2019) and ELCOM (Hodges et al., 2000). Several of these hydrodynamic models are coupled to biogeochemical models to allow for prediction of water quality. In the case of hindcast applications, the complex and time-consuming setup and calibration procedure, of these models, can result in a significant time lag (months to years) between when a project is initiated and when the model results are communicated to stakeholders, which severely limits the utility of computational models for management decision making. For better application of these powerful tools, rapid monitoring and forecast systems should be established.

In addition to the significant effort required to setup and calibrate models, other hurdles exist such as data-sharing agreements between the agencies collecting forcing/validation data and those running the models. For example, the US National Oceanic and Atmospheric Administration (NOAA) Great Lakes Coastal Forecasting System (Chu et al., 2011; Anderson et al., 2018), is a comparatively large-budget multi-institutional (NOAA-GLERL and U. Michigan-CIGLR) project that predicts water levels, temperature profiles, currents, and wave heights over a 120-h timeframe in the five Laurentian Great Lakes and connecting channels, using FVCOM on a 3D unstructured grid with 30-2000 m horizontal resolution. Similarly, meteolakes.ch (Baracchini et al., 2020), applies Delft3D with short-term forecasts (4.5 days) of Swiss lakes, under a data sharing agreement between Swiss Federal Institute of Aquatic Science and Technology (EAWAG), École Polytechnique Fédérale de Lausanne (EPFL) and MeteoSwiss.

With the present online proliferation of near real-time data from lake observation buoys (e.g., https://www.ndbc.noaa.gov/; https://www.glos.us/; https://marees.gc.ca/eng/) and high-resolution meteorological forecasts (https://dd.weather.gc.ca/model_gem_global/), data collection, assembly of forcing files, model execution, post processing and online communication of model results can be automated to near real-time, without a need for data-sharing arrangements. This drastic improvement in workflow efficiency can allow for the development of specific simulations tailored to meet diverse lake-management needs (e.g., high-resolution nearshore grids, spill modelling, fisheries research, beach closures, and optimization of treatment or source water monitoring strategies). In the present study we develop a pilot operational lake forecasting system for Lake Erie. The system is called COASTLINES (Canadian cOASTal and Lake forecastINg modEl System) and it uses Python-based wrapper code, that processes publicly available real-time data to execute a hydrodynamic lake model and produce web-based real-time products to communicate the results. The objective of this paper is to assess the accuracy of the model in forecasting water levels and temperature fields, compared to traditional hindcast applications of numerical models. This will determine the reliability of the model for short-term water management decision support for government agencies and other stakeholders. The data and methods are presented in Section 2, with an overview of COASTLINES including the workflow and a description of the implementation for a large lake (i.e., Lake Erie). The results are described in Section 3, including validation and evaluation of the forecast variables (water levels and temperatures), showcasing the short-term predictive ability of COASTLINES over timescales of 24-h and 240-h. A discussion of the forecast performance of COASTLINES with other operational platforms of lakes (GLCFS, meteolakes.ch) and hindcast simulations is provided in Section 4, including an analysis of the advantages and potential bias and uncertainty.

2 Data and methods

2.1 Study site

Lake Erie, the shallowest lake of the Great Lakes with a mean depth of 19 m. Lake-wide hydrodynamics predominantly exhibits free surface and current oscillations from the 14-h barotropic seiche (Hamblin 1987; Boegman et al., 2001). The lake morphometry consists of distinct, yet interconnected western, central, and eastern basins (Fig. 1), each with its own water quality concerns: The 11-m deep western basin is typically well mixed and has frequent harmful algae blooms related to climate-driven meteorological forcing (Michalak et al., 2013). The ephemeral stratification in late summer (Loewen et al., 2007) regulates vertical biogeochemical fluxes (Boegman et al., 2008). The 20-m deep central basin is prone to large-scale hypolimnetic hypoxia (Scavia et al., 2014). Hydrodynamics are governed by an internal Poincaré wave (Bouffard et al., 2012; Valipour et al., 2015) and a bowl-shaped depression of the summer thermocline, which influence the oxygen budget (Beletsky et al., 2012; Bouffard et al., 2014). The 65-m deep eastern basin has nearshore water quality concerns from *cladophora* (Higgins et al., 2006) and ecosystem engineering by dreissenid mussels (Hecky et al., 2004). Hydrodynamics of this region are controlled by the coastal internal Kelvin wave (Valipour et al., 2019).

https://doi.org/10.5194/gmd-2021-34
Preprint. Discussion started: 29 March 2021

Geoscientific Model Development
Discussions

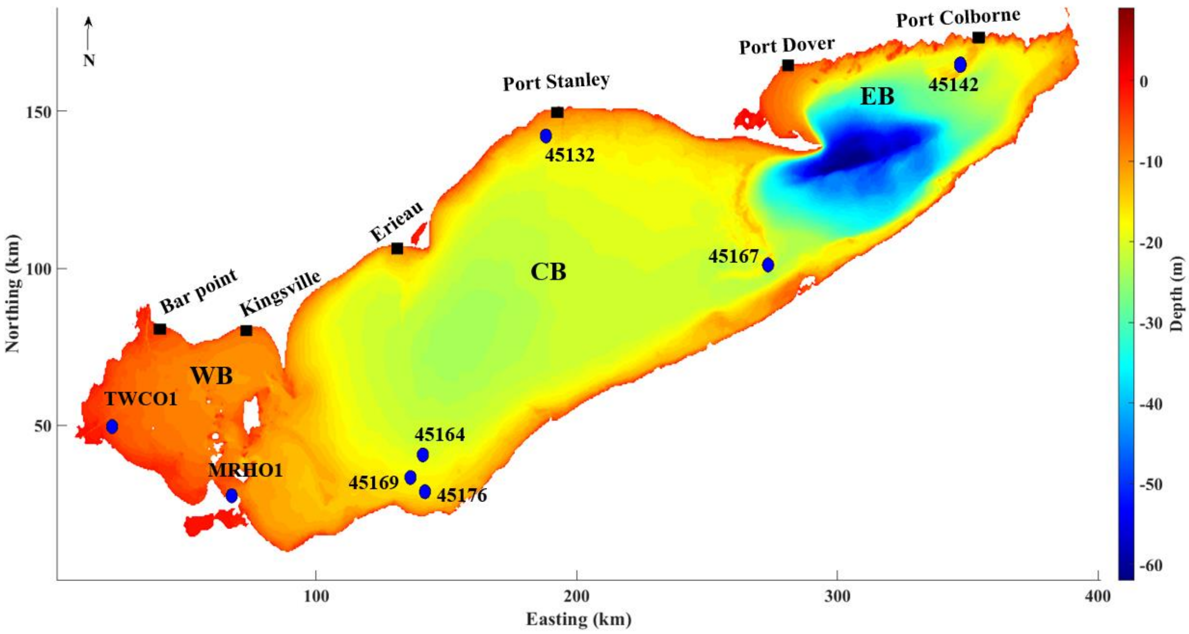

Fig.1 Map of Lake Erie showing the bathymetric depths and observation sites. The bathymetric map is at the resolution of the 500 m grid applied in the model. The western, central, and eastern basins are labeled as WB, CB, and EB, respectively. Blue circles indicate lake buoys and black squares indicate water level gauges.

2.2 Model description

COASTLINES applies the three-dimensional Aquatic Ecosystem Model (AEM3D, HydroNumerics Pty Ltd.). This model solves unsteady 3D Reynolds-averaged Navier-Stokes equations for incompressible flow based on Boussinesq and hydrostatic approximations. The advection of momentum in the model is based on the Euler-Lagrange method with a conjugate-gradient solution for the free-surface height (Casulli and Cheng, 1992), and a conservative ULTIMATE QUICKEST discretization scheme is used for advection of scalars (Leonard, 1991). AEM3D is a parallel version of the commonly applied Estuary and Lake Computer Model (ELCOM; Hodges et al., 2000). ELCOM has been applied to Lake Erie to simulate currents and seasonal circulation (León et al., 2005), the internal Poincaré (Valipour et al., 2015) and Kelvin waves (Valipour et al., 2019), ice cover (Oveisy et al., 2012) and the response of the thermal structure, in Lake Erie, to air temperature and wind speed changes (Liu et al., 2014). ELCOM has been coupled with the biogeochemical CAEDYM model to simulate Lake Erie phytoplankton and nutrients (León et al., 2011), the response of hypoxia (Bocaniov and Scavia 2016) and algae blooms (Scavia et al., 2016) to nutrient load reductions. Recent applications of AEM3D include a study of the water level in Lake Arrowhead, California (Saber et al., 2020), ice cover in Lake Constance (Caramatti et al., 2019) and pollutant transport in Lake St. Clair (Madani et al., 2020).

https://doi.org/10.5194/gmd-2021-34
Preprint. Discussion started: 29 March 2021

Geoscientific Model Development Discussions

2.3 Model setup and meteorological forcing variables

To adequately resolve the coastal boundary layer (~ 3 km width; Rao and Murthy, 2001) and basin-scale internal waves (Poincaré (16.8 h) and Kelvin waves), the bathymetry of Lake Erie (https://www.ngdc.noaa.gov/mgg/greatlakes/erie.html) was discretized into a 500 m × 500 m horizontal grid, which is ~10 % of the internal Rossby radius (Schwab and Beletsky, 1998). The lake was discretized into 45 vertical layers, with fine resolution (0.5 m) through the surface layer, metalimnion and bottom of the central basin, and coarse layers (5 m) through the hypolimnion of the deeper eastern basin to the maximum depth of 64 m.
The model was 'cold started' with the surface water temperature observed at station 45142 and MHRO1 on day of year (day) 99, 2020, at a time when the spring turnover and stratification is minimal, and the model has been running continuously since that time. The model time step is dt = 300 s to satisfy the CFL (Courant-Friedrichs-Lewy) condition for internal waves, which is CFL = (Hodges et al., 2000).
The model is driven by meteorological forcing including wind speed, wind direction, air temperature, shortwave solar radiation, relative humidity, air pressure, and net longwave radiation. The net longwave radiation is computed internally within AEM3D from cloud cover and modelled surface temperature. In order to address the spatial variability of meteorological conditions across the lake, the computational domain was forced with meteorological data on horizontal grids at 15 km (https://dd.weather.gc.ca/model_gem_global/15km/) and 25 km (https://dd.weather.gc.ca/model_gem_global/25km/) resolution using meteorological forecasts from the Environment and Climate Change Canada Global Deterministic Forecast System (GDPS). This resulted in 31 and 23 meteorological sections for the 15 km and 25 km models, respectively. Wind speed, direction, air temperature, relative humidity, air pressure, dew point, and cloud cover are direct outputs from GDPS, with solar radiation calculated based on dew point and air pressure (Meyers and Dale 1983; Appendix C. in Gaudard et al., 2019). The meteorological forecast has an output timestep of 3-h and a forecast length of 240 hours. The .GRIB2 meteorological data were retrieved via 'urllib' library in Python and formatted into AEM3D input files using the nctoolbox in MATLAB.
In this pilot application, the Lake Erie inflows and outflows, which roughly balance, are neglected, however evaporation and precipitation are accounted for in the water balance.

2.4 Observations, implementation and model validation

The water levels and temperatures simulated by COASTLINES were validated using both in situ and satellite observations. Near real-time water level data was used from six stations along the Canadian coastline, which reported hourly observations (Bar Point, Kingsville, Erieau, Port Stanley, Port Dover, and Port Colborne; Fig. 1; Table 1), retrieved from Fisheries and Oceans Canada (https://marees.gc.ca/eng/find/zone/44). The data are parsed using the 'BeautifulSoup' library in Python and saved as .csv files (Appendix A1), to be read with MATLAB for model validation. The observations showed higher fluctuations in the western (Bar Point and Kingsville) and eastern (Port Dover and Port Colborne) basins (Fig. 1). Thus, we quantify the water level forecast capability in terms of the Root Mean Square Deviation (RMSD) and Relative Error (RE):

https://doi.org/10.5194/gmd-2021-34
Preprint. Discussion started: 29 March 2021

$$RMSD = [\frac{1}{N}\sum_{i=1}^{N}(x_i - y_i)^2]^{1/2}, \quad (1)$$

$$RE = 100\frac{RMSD}{log.\ mean(daily\ range)}, \quad (2)$$

where x_i and y_i (i = 1, 2, 3, ... N) are the model and observed water level timeseries and N is the number of samples. RMSD is the absolute error of the model against the observation. The difference between the observed daily minimum and maximum value was defined as the daily water level fluctuation range, and the RE is the ratio between RMSD and lognormal mean of daily range over April to September 2020. Given that our study focusses on a 240-h forecast, RE is able to characterize the forecast bias, regardless of the instantaneous water level position. Eight in situ lake buoys, distributed over the nearshore areas of three basins (Fig. 1; Table 1), provided near real-time data through the Great Lakes Observing System (GLOS: https://www.glos.us/) and National Data Buoy Center (NDBC: https://www.ndbc.noaa.gov/) portals. The text-based NDBC observations in are parsed using the 'BeautifulSoup' Python library (Appendix A2), and the GLOS observations are retrieved using 'webdriver' from the 'selenium' Python library. All the lake buoy observations are saved as .csv files and read into MATLAB for post-processing. This process is repeated for each station. Attempts to retrieve missing variables results in run-time errors.

The lake buoys are deployed from April or May through mid-October, spanning the spring/fall turnovers and seasonal summer stratification periods. However, due to COVID-19 related delays in instrument deployments in 2020, only two buoys located offshore of Cleveland near the water intake crib (station 45176 and station 45164) were equipped with thermistor chains to monitoring temperature profiles. The other six buoys provide air and surface water temperature as well as wind speed and direction observations applied for lake surface temperature (LST) and meteorological forecast validation. Satellite-based observations of LST were obtained from the Great Lakes Surface Environmental Analysis (GLSEA2), which is derived from NOAA CoastWatch AVHRR (Advanced Very High-Resolution Radiometer) imagery and updated on NOAA GLERL website (https://coastwatch.glerl.noaa.gov/erddap/files/GLSEA_GCS/). GLSEA2 produced daily observations, with 2.6 km resolution, from the cloud-free portions of the satellite images (Schwab et al., 1999). The data are in netCDF format, which is retrieved using the 'BeautifulSoup' library and 'webdriver' from 'selenium' (Appendix A3).

We quantify the temperature forecast capability using the statistical measures of RMSD (eq. 1) and Mean Bias Deviation (MBD):

$$MBD = 100\frac{\frac{1}{N}\sum_{i=1}^{N}(x_i - y_i)}{\frac{1}{N}\sum_{i=1}^{N}y_i} \quad (3)$$

In *spatial* MBD and RMSD (s-MBD and s-RMSD), x_i and y_i are the model and observed temperature in each grid, and N is the total number of grids. In *timeseries* MBD and RMSD (t-MBD and t-RMSD), x_i and y_i are the model and observed temperature at each sample time, and N is the total number of samples.

Table 1
Details of field stations with water level gauges and lake buoys.

Station	Parameter	Sampling interval (min)	Depth of measurement (m)
Bar Point	Water level	60	Surface
Kingsville	Water level	60	Surface

https://doi.org/10.5194/gmd-2021-34
Preprint. Discussion started: 29 March 2021

Erieau	Water level	60	Surface
Port Stanley	Water level	60	Surface
Port Dover	Water level	60	Surface
Port Colborne	Water level	60	Surface
TWCO1	Temperature	10	Surface
45005	Temperature	10	Surface
45176	Temperature	10	1, 3, 4, 6, 7, 9, 10, 12, 14, 15
45169	Temperature	30	surface
45164	Temperature	60	1, 2, 4, 6, 8 10
45132	Temperature	60	Surface
45167	Temperature	10	Surface
45142	Temperature	60	Surface

2.5 System operation

The COASTLINES operational forecast system is run on a local server supported by Queen's University (Kingston, Canada). The COASTLINES workflow is presented in Fig. 2. The system consists of input data acquisition and preparation, 24-h hydrodynamic simulations, 240-h hydrodynamic simulations, validation against in situ observations, and uploading the model forecasts and validation to the web platform. Given that the standard deviations of meteorological forecast variables increase with forecast lead time (Buehner et al., 2015), we separated the 24-h and 240-h forecast simulations, with both performed daily. The model advances daily according to the 24-h forecast simulation and generates 're-start' files. These files are then used to initiate 240-h forecast simulations and the 24-h simulations for the next day. The input files for the new 240-h forecast simulations are replaced by the new input files with the 240-h meteorological forecast generated each day. Daily 24-h and 240-h forecast model outputs are compared against observations, respectively, to evaluate the forecast performance against forecast length. Automation of the processing tasks in the system is performed by Python scripts triggered by the Windows Task Scheduler every 24-h at midnight. The online meteorological forecast data are retrieved from GDPS once updated at around 3 am EST. Forcing variables are formatted in MATLAB, called by the Python scripts once the meteorological forecast data from GDPS are retrieved. The 24-h simulation and 240-h simulations take 0.5 h and 4 h to complete, respectively, on a 32-core XEON workstation. The observed data, including water level from gauge stations, water temperature from lake buoys and satellite imageries are scraped at 8 am, followed by post-processing in MATLAB to validate model output, calculating statistical metrics (RMSD, MBD). The results are exported to Google sheets and published to the COASTLINES website (e.g., Appendix B). Global coverage of the GDPS forecasts enables this operational system to be readily implemented at other sites where lake bathymetry, boundary flows and in-situ validation data are available.

https://doi.org/10.5194/gmd-2021-34
Preprint. Discussion started: 29 March 2021

Geoscientific Model Development Discussions
Open Access
EGU

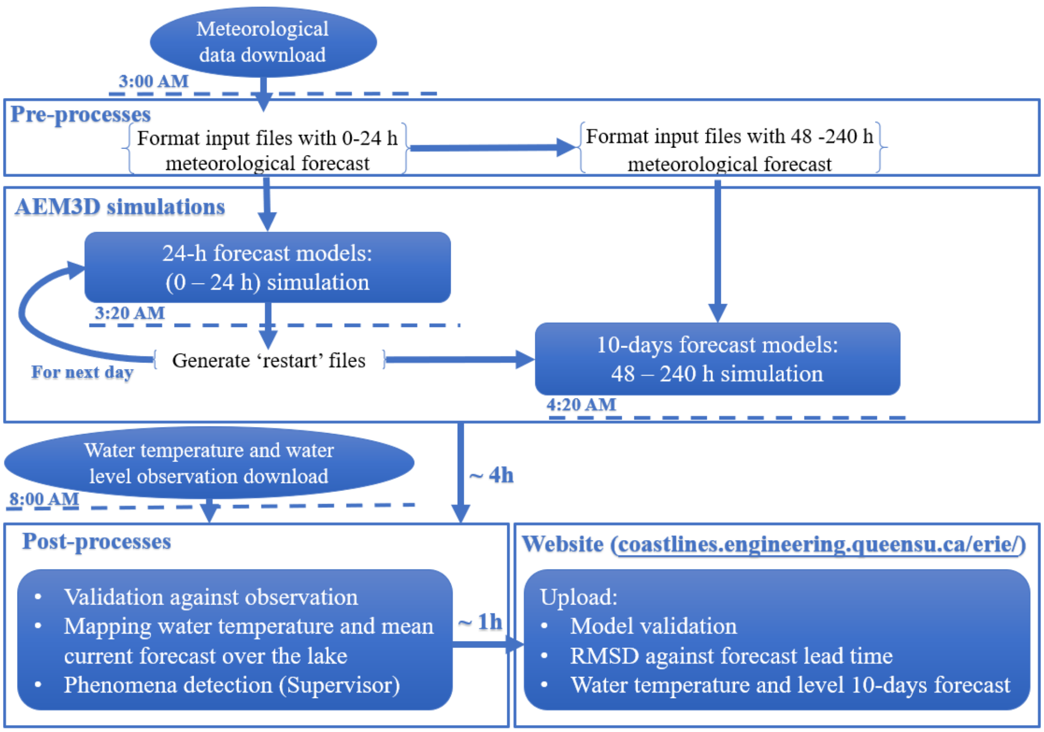

Fig. 2 Daily Python workflow and automated processes in the COASTLINES operational system as performed on the local server.

3 Results

The COASTLINES water level and temperature forecasts have been operational since April and July 2020, respectively. The 24-h and the 240-h forecast of water levels from the 15 km and 25 km resolution models were validated against real-time gauge station observations. The statistical metrics of water level RMSD and RE were ensembled over April to September 2020. The 24-h and the 240-h forecast of LST and temperature profiles from the models were also validated against real-time lake buoys and daily averaged satellite imageries. The timeseries and spatial MBD and RMSD (t-RMSD, t-MBD and s-RMSD, s-MBD) were ensembled over July to September 2020.

3.1 Water level

The Relative Error (RE) of the forecast water level generally increases with forecast time when averaged over April to September 2020; the 24-h forecast error being ~ 40% at all six gauge stations (Fig. 3 a, c, e, g, i, k). Given the large water level fluctuation at Port Colborne (Fig. 3 l), the 240-h forecast RE is highest at this station, exceeding 70% (Fig. 3 k). Of the six gauge stations reported in this study, those at the western (Bar Point and Kingsville) and eastern (Port Dover and Port Colborne) ends of Lake Erie longitudinal axis had the largest water level fluctuations, resulting from the predominant south-westerly winds generating strong wind set-up and surface seiches (Fig. 3 b, d,

https://doi.org/10.5194/gmd-2021-34
Preprint. Discussion started: 29 March 2021

f, h, j, l). The lognormal means of the daily range in water level at the six gauge stations are 0.21 cm (Bar Point), 0.16 cm (Kingsville), 0.07 cm (Erieau), 0.10 cm (Port Stanley), 0.15 cm (Port Dover), 0.17 cm (Port Colborne). The 24-h forecasts show qualitative agreement with observations in phase and magnitude (Fig. 4). The 24-h forecasts reproduce the dramatic surface seiches induced by westerly winds > 15 m s^{-1} (Fig. C2) on day 251 (RMSD < 0.1 cm), especially the obvious water level fluctuations at stations in the western and eastern basins (Fig. 4 a, b, e). However, the prediction of water level at Bar Point showed large bias (Fig. 4 f), with the model overestimating the decrease in water level. This error may result from neglecting the large Detroit River inflow, which occurs near Bar Point. The uncertainty in the model forecast, which increased with the range of the daily fluctuation, was captured by the ensemble 24-h forecast RE over April to September (the shaded areas in Fig. 4). Overall, the confidence interval of the 24-h forecast can include most of the discrepancies between the observations and the model results.

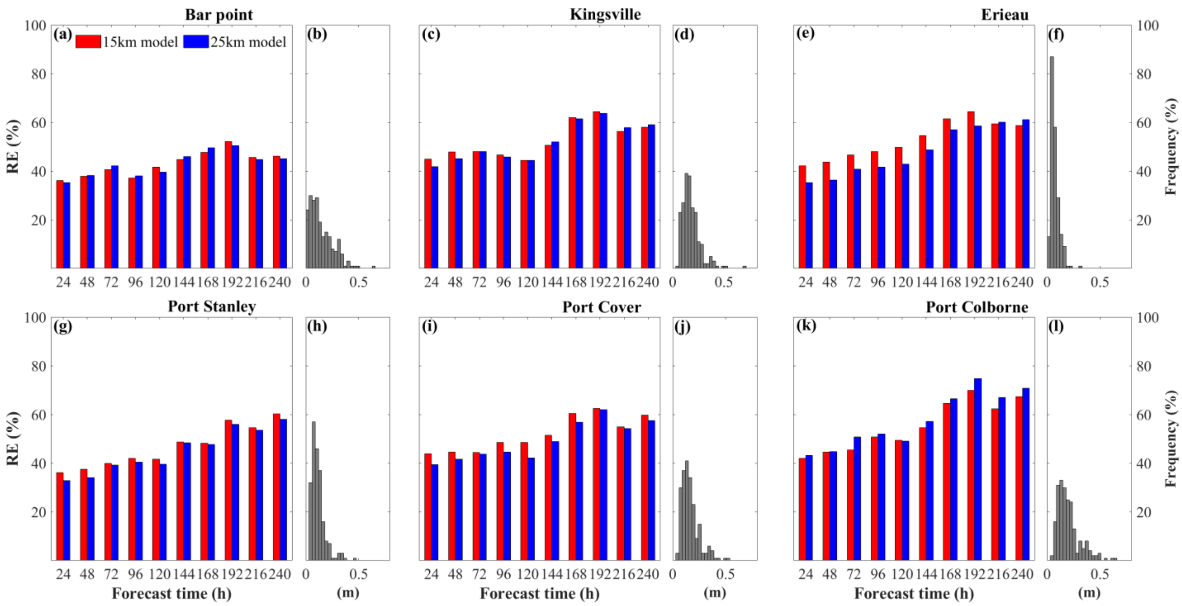

Fig. 3 Relative error (RE) in water level predictions against forecast time at six stations (a, c, e, g, i, k). Panels (b, d, f, h, j, l) are the corresponding frequency distribution of lognormal means of the daily water level fluctuation range (x-axes, unit in meter) at Bar Point, Kingsville, Erieau, Stanley, Port Dover, Port Colborne, respectively.

https://doi.org/10.5194/gmd-2021-34
Preprint. Discussion started: 29 March 2021

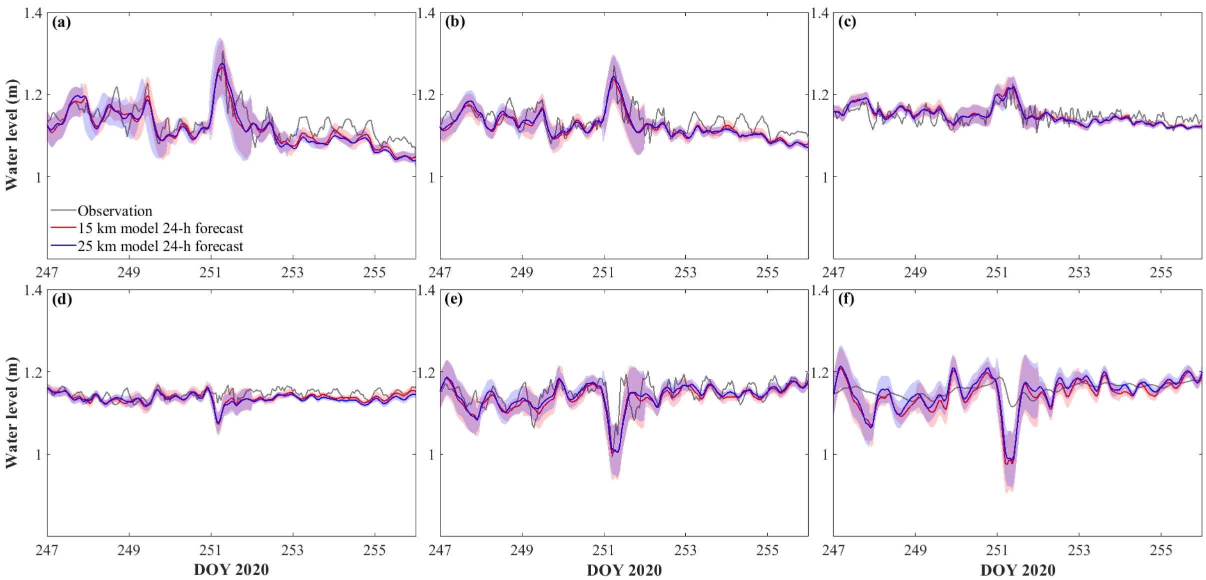

Fig. 4 Comparison between observed and stitched 24-h forecast modeled water level at (a) Port Colborne, (b) Port Dover, (c) Port Stanley, (d) Erieau, (e) Kingsville, and (f) Bar Point. The shaded areas show the confidence interval of the 15 km model (red shading) and the 25 km model (blue shading), as given by the ensemble 24-h RE in Fig. 3.

Timeseries validations for the 240-h model forecast (Fig. 5) include confidence intervals from the ensembled RE (Fig. 3). As shown, the forecast began 6 days in advance of the large surface seiche event on day 251 and predicted the seiche to crest at Port Colborne 1-2 h ahead of the observations, and to trough at Kingsville 1-2 h behind the observations (Fig. 5 a, c). Damping of the seiche oscillations (~144 hours in the future) was excessive, with the water levels being underestimated and the phase shifted by approximately 12 hours (Fig 5. a, b). Despite the wide confidence intervals, due to the increasing RE with forecast time, large bias existed after the seiche event (forecast time >168 hours). When the forecast initiation was close to the event (3 days before), the prediction of seiche phase was more accurate (Fig. 5 d, e, f). However, the seiche decay still had a 12-h phase shift. The discrepancies in seiche amplitude (< 0.1 m) were within the confidence intervals of the models.

https://doi.org/10.5194/gmd-2021-34
Preprint. Discussion started: 29 March 2021

Geoscientific Model Development
Discussions
Open Access
EGU

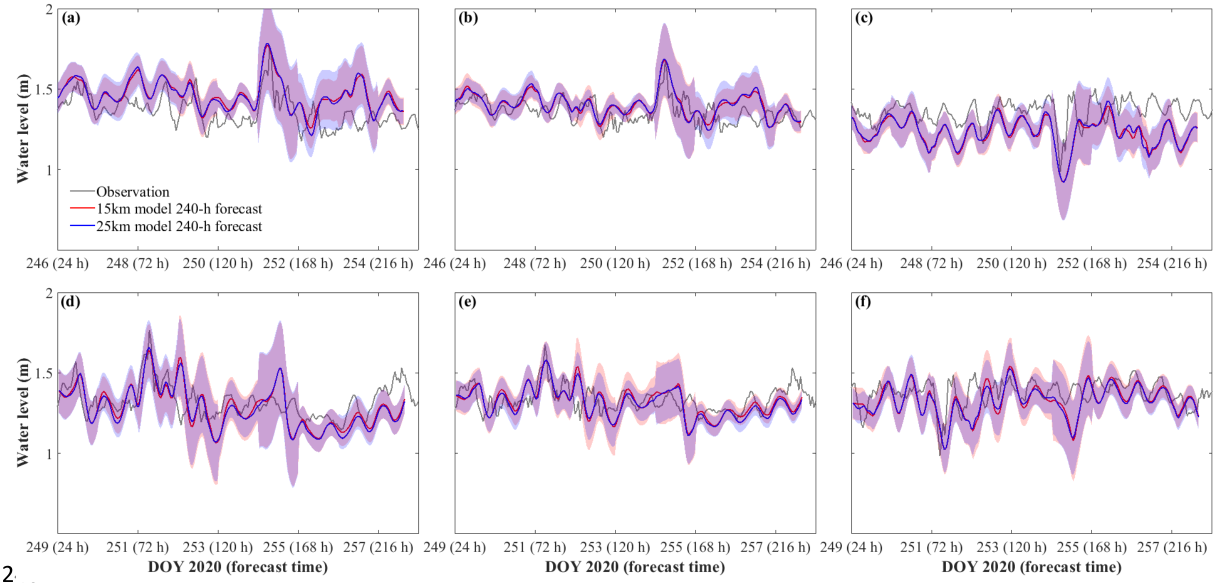

Fig. 5 Comparison between the observed water level and 240-h forecast initiated on day 245 (a, b, c) and day 248 (d, e, f) at Port Colborne, Port Dover, and Kingsville, respectively. The shaded areas show the confidence interval of the 15 km model (red shading) and the 25 km model (blue shading), as given by the ensemble 240-h RE in Fig. 4.

3.2 Water temperature

3.2.1 Lake Surface temperature

Using satellite-based and lake buoy-based observations, we evaluated the LST forecast (Fig. 6). The 24-forecast captured the seasonal variation of LST, particularly the rapid increase in temperature on days 180-190, and the gradual decrease in temperature after day 240; at all eight stations. However, the forecast overestimates the LST in July with 3-5 °C (days 180-210), especially at STN 45167 and 45142. Due to the 3-h delivery interval associated with the meteorological forecast data, the forecast model was insensitive to temperature fluctuations over shorter timescales, as recorded by the lake buoys, and it underestimated the sudden decrease in temperature near day 220 and 255 at STN 45005.

Overall, the t-MBD and t-RMSD, over these eight stations, were ~6% and 1.4 °C (15 km model) and ~5% 1.3 °C (25 km model), respectively (Table 2). The average s-MBD and s-RMSD over the 50 days from July-September were ~4% and 1.2 °C, respectively, for both 15 km and 25 km resolution models.

https://doi.org/10.5194/gmd-2021-34
Preprint. Discussion started: 29 March 2021

Geoscientific Model Development
Discussions
Open Access
EGU

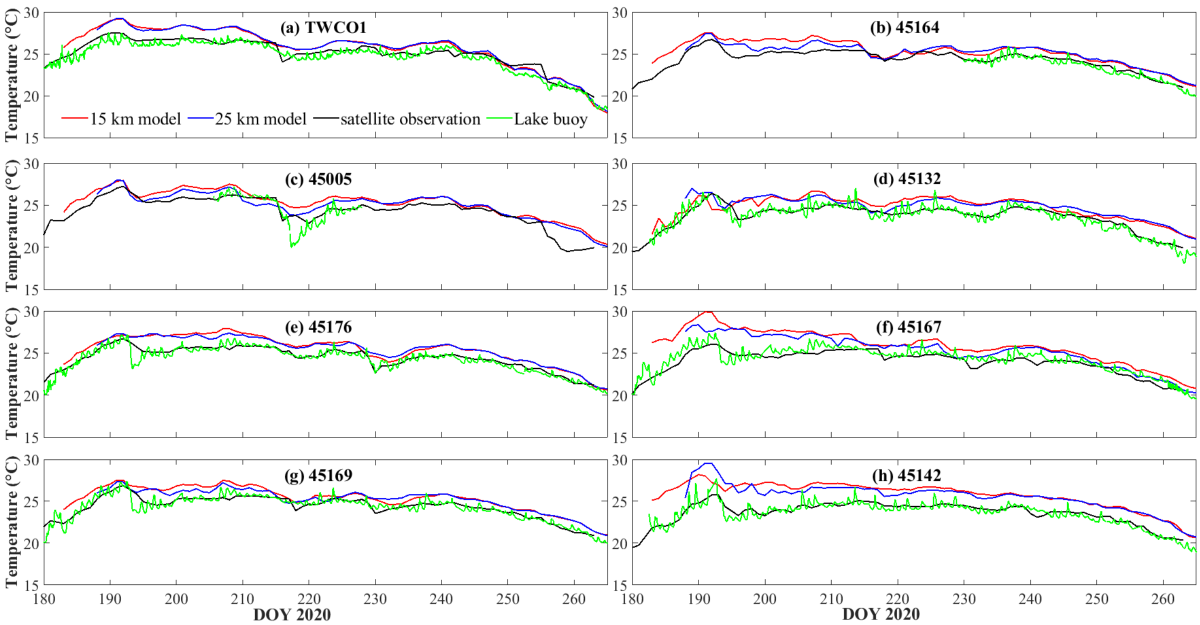

Fig. 6 Comparison between the stitched 24-h forecast and observed lake surface temperature (LST) at 8 stations (a) TWCO1, (b) 45164, (c) 45005, (d) 45132, (e) 45176, (f) 45167, (g) 45169, and (h) 45142. The green lines are timeseries observations from lake buoys, the black lines are daily observations derived from satellite imagery.

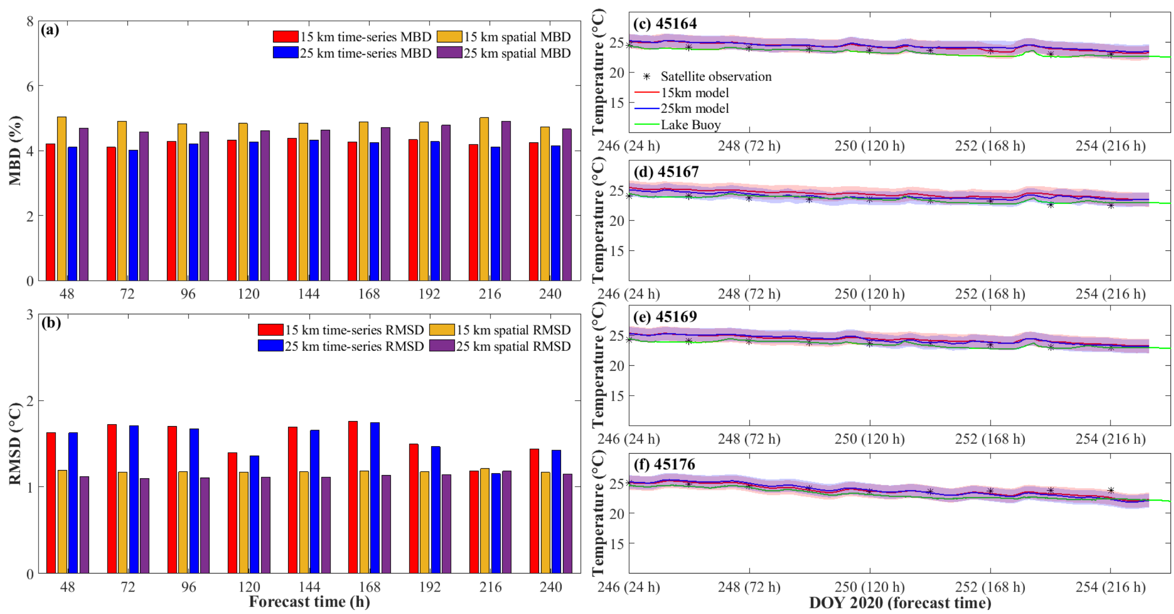

Fig. 7 (a) Mean-Bias Deviation (MBD) against forecast time; (b) Root-Mean-Square Deviation (RMSD) against forecast time. (c-f) Timeseries of 240-h forecast and observed LST at stations 45164, 45167, 45169, 45176, respectively, and daily averaged satellite LST (black asterisks). The confidence interval (shaded areas) in (c-f)

https://doi.org/10.5194/gmd-2021-34
Preprint. Discussion started: 29 March 2021

represents the uncertainty of the 240-h forecast model through the timeseries RMSD with the forecast time (panel b).

The 240-h forecast MBD and RMSD, surprisingly, do not show an increase in error with forecast time (Fig. 7 a, b). Both t-MBD and s-MBD, over the 240-h forecast, are ~4-5%, with s-MBD 0.5-1% higher than t-MBD. Although both 240-h s- and t-RMSD are under 2 °C, the t-RMSD show the fluctuation with forecast time to be higher than s-RMSD. Both timeseries observations from lake buoys and daily averaged observations from satellite imagery fall into the forecast confidence interval based on the 240-h t-RMSD (Fig 7 c-f).

Spatial comparisons of satellite-based observations and to the 24-h, 48-h, 120-h, 168-h surface temperature forecasts illustrate that the forecast system captured the cooling of the lake surface in late summer (Fig. 8). Without river inputs, which adjust more rapidly to air temperatures (~3 d) compared to deeper lake waters, the model predicted lower surface temperatures in coastal regions of the western basin, compared with the satellite observations (Fig. 8 e, f, g, i, j, k). The 24-h and 48-h forecast showed cold water along the northwest shoreline of the central basin with a cold bias ~ 2 °C; this may be up-welling hypolimnetic water (see following Discussion 4.2). Further comparisons between model predictions and satellite-based observations of LST can be found in the Supporting material (Fig. D1-2).

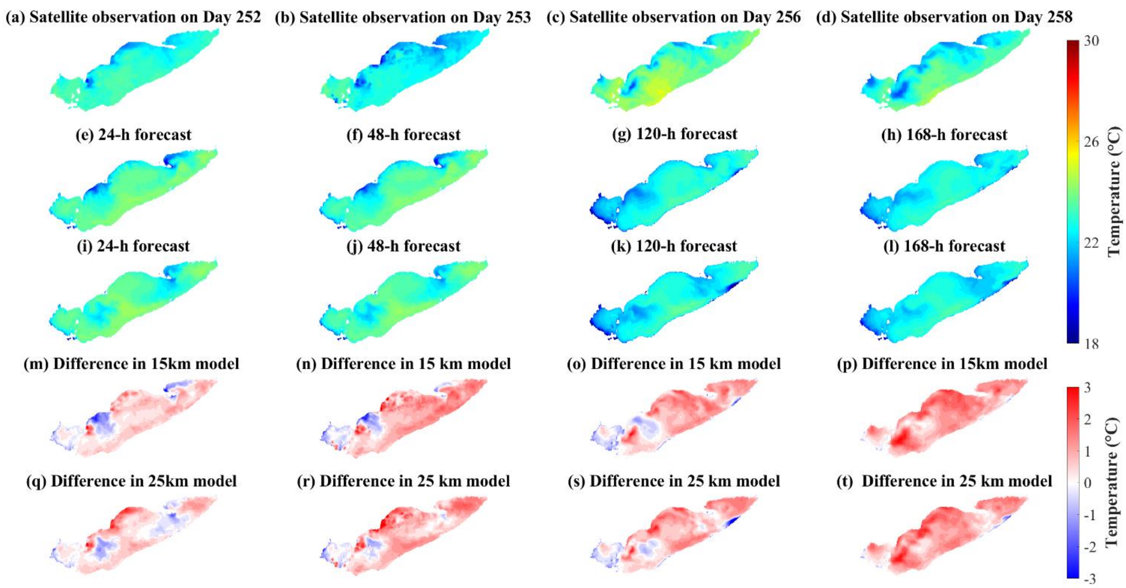

Fig. 8 Comparison of lake surface temperature from (a-d) satellite observations, (e-h) 15 km model forecast, and (i-l) 25 km model forecast during late summer. The models were initiated on day 251 The difference between observations and models are shown in (m-t).

3.2.2 Thermal structure

The three-dimensional structure of the AEM3D model applied in COASTLINES enables the prediction of the thermal structure in the lake. On 15 Jun. 2020 (day 168), a rapid drop (~ 6°C) in surface temperature, was recorded by the

https://doi.org/10.5194/gmd-2021-34
Preprint. Discussion started: 29 March 2021

thermistor at STN 45176, and predicted by the stitched 24-h COASTLINES model (15 km grid) (Fig. 9 a, b). The timing and intensity of this up-welling event were accurately forecast, but before and after the upwelling event, the mixed layer depth was modelled to be deeper than observed; perhaps a result of spurious numerical diffusion resulting from the thermocline swashing along the stair-step z-level grid at the lake perimeter. The 240-h forecast model was not yet operational at this time.

Both the 240-h 15 km and 25 km resolution forecasts predicted the down-welling event on 11 Jul. 2020 (day 193) at STN 45176 (Fig. 10). The forecasts were initiated 7 days before the event (day 187), successfully predicting when warm surface water down-welled toward the bed, displacing the thermocline (Fig. 10 b, c), but the 15 km resolution underestimated the intensity of this down-welling, predicting thermocline recovery on day 193. The forecast initiated 5 days before the event (day 189) presented a more accurate prediction with the down-welling persisting over 2 days (Fig. 10 d, e) – as observed (Fig. 10 a).

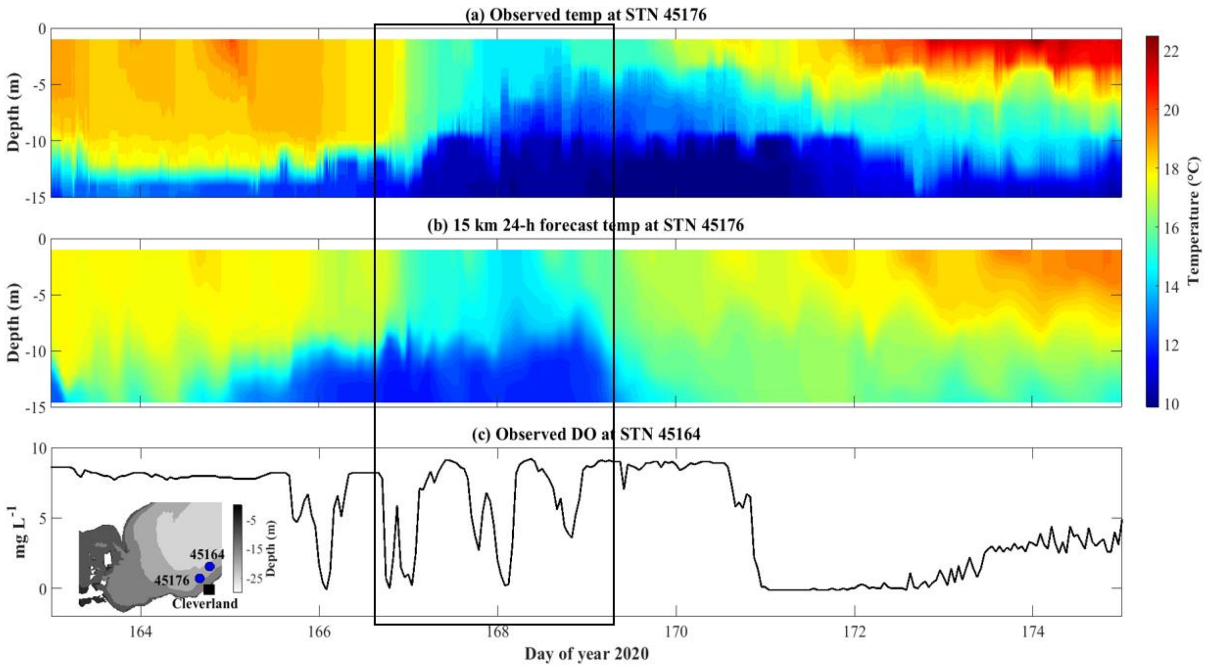

Fig. 9 Temperature profile comparisons between (a) observations and (b) stitched daily 24-h forecasts from the 15 km resolution model at station 45176. (c) Observed dissolved oxygen concentration at station 45164 from lake buoy (https://www.glos.us/). The inset image shows the bathymetry and locations of lake buoys. The black square indicates the timing of the up-welling event.

https://doi.org/10.5194/gmd-2021-34
Preprint. Discussion started: 29 March 2021

Geoscientific Model Development Discussions
Open Access
EGU

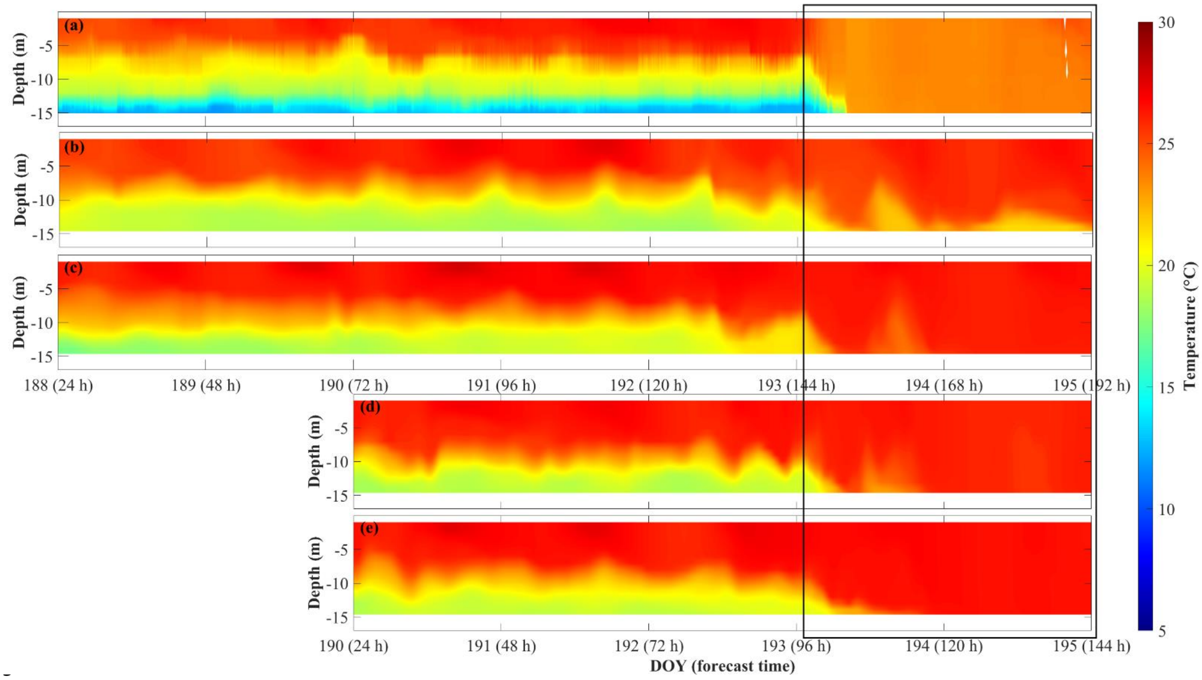

Fig. 10 Comparisons of (a) observed temperature profile, (b, d) 240-h 15 km resolution modeled, and (c, e) 240-h 25 km resolution modeled temperature profiles at STN 45176. The forecast models were initiated on day 187 (b, c), and day 189 (d, e). The black square indicates the down-welling event.

Table 2
Statistical measures of t-MBD (Mean-Bias Deviation) and t-RMSD (Root-Mean-Square Deviation) between the 24-h forecast model and observations of water temperature.

Station	RMSD (°C)		MBD (%)	
	15 km model	25 km model	15 km model	25 km model
45176	2.6	2.6	6.8	6.8
45164	1.8	2.1	2.2	2.3
45132	1.5	1.5	5.5	5.7
45142	2.4	2.1	9.9	8.8
45167	1.2	1.1	4.6	4.0
45169	1.3	1.2	4.7	4.6
TWCO1	1.0	1.0	3	1.9
45005	1.2	1.1	8.2	7.9

4 Discussion

4.1 Bias and uncertainty

The 240-h COASTLINES forecast is longer than the other operational lake forecast systems (GLCFS and meteolakes.ch) and is the only one forced with open-access meteorological data that has global coverage. GLCFS provides 48-h water level forecasts with RMSD ~0.12 m at the Buffalo gauge and ~0.14 m at the Toledo gauge, corresponding to RE ~ 60% and 51%, respectively (O' Connor et al., 1999; Trebitz, 2006); using the older 4 km grid

https://doi.org/10.5194/gmd-2021-34
Preprint. Discussion started: 29 March 2021

implementation of POM, as opposed to the newer unstructured grid FVCOM GLCFS. COASTLINES gives better 48-h forecast performance (RE ~ 40 %) for water levels at six gauge stations.

Benefitting from a smaller domain, finer resolution meteorological input (~2.2 km) and data assimilation, the 4.5-day LST predicted by meteolakes.ch has RMSD = 0.8 °C (Baracchini et al., 2020), whereas COASTLINES predicts the 120-h (5 d) LST with RMSD ~ 1.7 °C. Given this small improvement in LST prediction, it is not clear if the added model complexity and computational cost, associated with data assimilation, justify a small improvement in simulated water temperature; particularly, when the objective of the present work is to develop a simple automated lake modelling system that can be readily to diverse field sites to suit management needs.

The AEM3D (formerly ELCOM) model employed in COASTLINES has shown skill in temperature hindcasts in the Great Lakes with RMSD ~ 0.9 – 3 °C in Lake Erie (Liu et al., 2014; Oveisy et al., 2012) and 1.5 – 1.9 °C in Lake Ontario (Paturi et al., 2012). The 24-h COASTLINES forecast predicts the water temperature with an average s-RMSD and t-RMSD < 2 °C at the surface (Table 2). Therefore, the forecasts are within ~1 °C RMSD in comparison to hindcasts, showing sufficient model skill for predictive simulations to aid lake management (e.g., movements of hypoxic water, fish thermal habitat, etc.).

The accuracy of the COASTLINES forecasts, relative to hindcasts using observed meteorological conditions, may result from the limited spatial resolution associated with historical meteorological data. Liu et al., (2014) applied uniform Lake Erie meteorological forcing over 4 zones and Valipour et al., (2019) utilized 6 zones, each spanning ~100 km. These included land-based observations, when there was no available lake buoy data, which induces error, especially in large shallow lakes (Hamblin, 1987). The comparatively high-resolution GDPS meteorological forecast was four to five times higher in horizontal resolution than used in the hindcast simulations, improving the representation of regional meteorological and climatological conditions in the model. For example, a spatially variable wind field is essential for simulating the mean surface circulation (Laval et al. 2003). In Lake Erie, the thermocline depth and hypolimnetic water temperature are sensitive to wind (Beletsky et al. 2012; Liu et al., 2014). The 3-h time interval between GDPS forecast dataset updates is much less than the 10-min interval associated with meteorological collected by lake-buoys for hindcasts (e.g., Leon et al., 2005) and so the coarse GDPS forecast resolution may alias temporal events, such as wind gusts (Fig. C1), inducing a potential source of bias and uncertainty in the hydrodynamic predictions. This is of particular concern in large shallow lakes, such as Lake Erie, where winds play the dominant role in driving water level fluctuations.

Comparisons between observed and forecast meteorological data at selected stations are shown in Appendix C (Fig. C1-5). The 24-h air temperature and wind speed forecasts had ~ 1.5 °C and ~ 2 m s^{-1} RMSD, respectively. However, in the 240-h forecast, the bias in meteorological forecast data, especially the wind forecast, increases with forecast time (Buehner et al., 2015). The 168-h forecast meteorological data overestimates wind speeds by up to 10 m s^{-1} (Fig. C4).

In addition to inaccuracy in meteorological forecasts, the discrepancies in simulating temperature profiles forecast may result from numerical diffusion arising due to the discrete nature of the vertical and horizontal grids. The simulated thermocline depth is overestimated (Fig. 9, 10), as occurred in applications of ELCOM with both higher (Nakhaei et al., 2019) and lower resolution (Paturi et al., 2012). COASTLINES has the potential to predictively simulate mesoscale physical processes, such as Kelvin waves (Bouffard and Lemmin, 2013; Valipour et al., 2019) and nearshore-offshore exchange (Valipour et al., 2019); however model performance is poor in nearshore areas, where topographic features remain poorly resolved (; their figure 3.14).

4.2 Prediction of coastal up-welling for fishery and drinking water management

The central basin of Lake Erie is vulnerable to hypoxia in the summer due to the thermal stratification and relatively large ratio of surface area to hypolimnetic volume. Associated fish kills events (10s of thousands) are regularly reported, including an event on north shore of the central basin in the late summer of 2012, which was presumably was caused by up-welling of cold anoxic water from the hypolimnion (MOE, 2012; Rao et al., 2014). Similarly, 1000s of freshwater drum were killed in a rapid warming event (~5 °C /week) in the western basin in 2020 (https://www.13abc.com/content/news/Hundreds-of-dead-fish-wash-up-in-Sandusky-Bay-571025541.html).
Shoreward advection of hypoxic water, from up-welling or internal waves also adversely affects source water quality at drinking water intakes (https://epa.ohio.gov), whereby high Fe and Mn or low pH, associated with hypoxia water require adjustments to treatment processes. This is particularly an issue along the Ohio coast of the central basin (Ruberg et al., 2008; Rowe et al., 2019).
The ability to predict these movements of hypolimnion water would aid management of both the Lake Erie fisheries and drinking water treatment. Here, we test the ability of the model to predict up-welling of cold bottom water in the region where the fish kill was observed in 2012. On days 249-253, 2020 (Fig. 8) strong southwesterly winds (~ 12 m s^{-1}; Fig. C2) were modelled and observed to create up-welling along the north shore, as expected from Ekman drift of the surface layer. The upwelled cold hypolimnetic water is shown near the coast of Erieau in satellite-based observations and the 15 km resolution model (Fig. 8 a, b, e, f). The depth-averaged water temperature and current circulation the in forecast results demonstrate that the up-welling process lasts several days (Fig. 11), with cold hypolimnetic water accumulating along north shore and strong eastward currents along the northern shoreline of the east central basin. The up-welling region matched that shown in a 2013 hindcast simulation (Valipour et al., 2019), revealing the hotspots of vertical transport of nutrients and anoxic hypolimnetic water.
Another up-welling event occurred near the Cleveland drinking water intake crib on days 167-170 (Fig. 9). This event was accompanied by simultaneous ~8 mg L^{-1} oscillations in the dissolved oxygen concentration (Fig. 9 c) at STN 45164 (~20 km away from STN 45176), followed by the dissolved oxygen concentration remaining hypoxic (< 2 mg/L) for 2 days. The COASTLINES model is shown to predict this event (section 3.2.2), which would provide notice for drinking water plane operators to implement additional treatment required for hypoxic water.
Future work, using the embedded iWaterQuality module (formerly CAEDYM) could extend COASTLINES to simulate biogeochemical parameters in Lake Erie (León et al., 2011), including dissolved oxygen (Bocianov et al., 2020).

https://doi.org/10.5194/gmd-2021-34
Preprint. Discussion started: 29 March 2021

Geoscientific Model Development Discussions

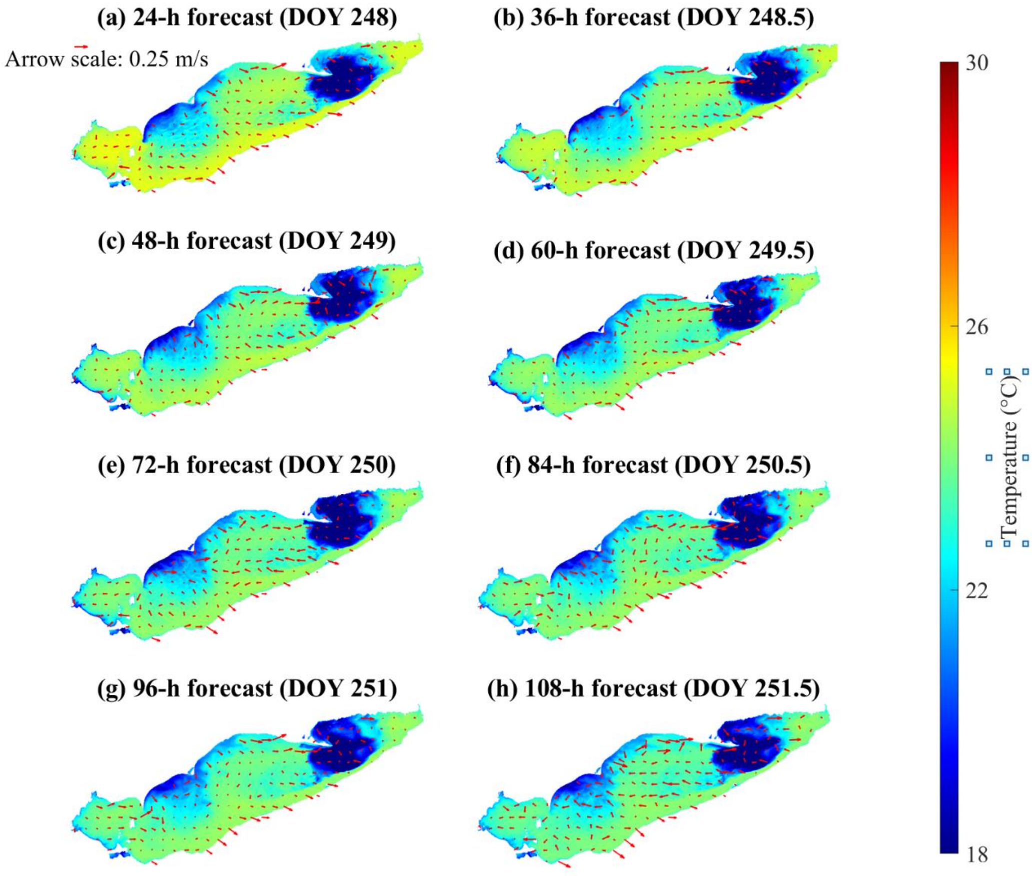

Fig. 11 Color maps showing the forecast depth-averaged temperature throughout the lake. The red arrows represent forecast depth-averaged currents. The model results are from the 240-h forecast model initiated on day 247.

4.3 Prediction of storm surge events for public safety

Due to its shallowness and long fetch aligned with the predominant southwest winds (Hamblin, 1979), Lake Erie has the largest daily range of water level amongst the Great Lakes (Trebitz, 2006). In each month of 2020, Lake Erie set new mean water level records (http://www.tides.gc.ca/C&A/bulletin-eng.html), causing the shoreline to be exposed to high risk from erosion and flooding and making the shoreline communities susceptible to costly damage and economic loss (e.g. https://www.lowerthames-conservation.on.ca/flood-forecasting/flood-notices/). Given the ability of COASTLINES to predict water level fluctuations induced by wind set-up (Fig. 3, 5), we test the ability of the model to act as a storm-surge warning system. This would assist early decision making during natural hazards (Gronewold and Rood, 2019). Due to the unpredictability and severity of water level fluctuations in Lake Erie, there

https://doi.org/10.5194/gmd-2021-34
Preprint. Discussion started: 29 March 2021

is currently a need to improve short-term water level forecasts and water level warning systems (Gronewold and Stow, 2014).

We forecast a storm event that occurred on 15 Nov. 2020, caused a dramatic water level increase (~1-1.5 m) in the eastern basin with strong surface currents (Fig. 12). The inset image, taken during the event, shows flooding in coastal areas. COASTLINES successfully predicted the phase of high-water level at Port Dover 72 hours in advance, but underestimated the increase of water level with over 0.5 m. The forecast operated 24 hours accuracy in water level prediction, with a difference <0.5 m from the observations (Fig. 12 d). Note that both forecasts missed the small (~0.5 m) seiche before the significant increase at the end of day 320, presumably due to the low temporal resolution of the meteorological forecast input or local topography near the gauge.

The hydrodynamic forecast output from COASTLINES could be further developed by enabling the coupled surface wave model SWAN (Booij et al., 1999). Coupled Delft3D-SWAN models have recently been applied in the development of a real-time predictive system for the coastal ocean and large estuaries (Rey and Mulligan, 2021).

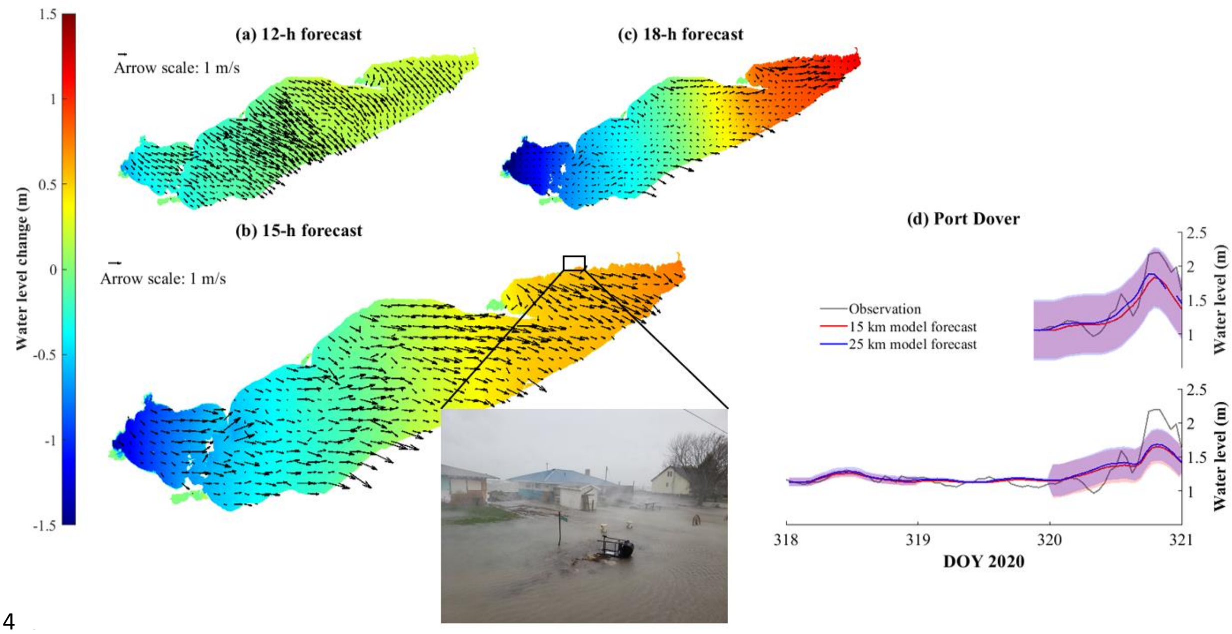

Fig. 12 Color maps showing the water level change compared to Nov 15th 00h from (a) 12 h, (b) 15 h, and (c) 18 h forecasts from 15 km resolution model. The black arrows are depth-averaged mean current fields. Panel (d) shows a comparison between forecast and observed water level at Port Dover. The upper panel shows the 24-h forecast, and the lower panel shows the forecast initiated on 12 Nov. 2020 (day 317). The shaded region indicates the confidence interval. The inset image (extracted from a footage by J. Homewood from Lower Thames Valley Conservation Authority) shows the flooding induced by the dramatic water level increase during this event. The two cottages shown in the images were demolished later in the afternoon.

https://doi.org/10.5194/gmd-2021-34
Preprint. Discussion started: 29 March 2021

Geoscientific Model Development
Discussions

5 Conclusions

We developed operational forecast system COASTLINES, using a Python-based wrapper code, to automate application of the three-dimensional hydrodynamic model AEM3D to Lake Erie. The resulting real-time and predictive lake modelling system employs a processing chain that retrieves online meteorological forecast data, prepares input files, executes the three-dimensional computational model and visualizes and compares model output with observations on the web-based platform. This operational system shows the feasibility of applying freely available meteorological forecasts, in situ buoy data and satellite images to drive and validate computational lake models. The favorable agreement between forecast model results and observed physical variables (e.g., water levels with RE ~ 40 % and temperatures with t-RMSD and s-RMSD < 2 °C) in Lake Erie demonstrates the ability of the forecast system to make predictions of hydrodynamic processes on time horizons up to 240-h that are as accurate as traditional hindcast simulations.

The near real-time updates to the web platform are an effective approach to rapidly disseminate forecast results to stakeholders. Examples we have investigated include at least 24-h prediction of: (1) up- and down-welling events that cause fish kills; up-welling events that bring hypoxic water to drinking water intake; and (3) coastal flooding events from storm surges.

The global coverage of the GDPS weather model allows this system to be extended to other lakes and water systems. To facilitate further development of open-access predictive modelling systems, agencies are encouraged to share observations in real-time through organizations such as GLEON (www.gleon.org) and GLOS (www.glos.us). This will enable extension of COASTLINES to include prediction of the biogeochemical variables that drive sediment transport, hypoxia and harmful algal blooms.

Code and data availability.

The observation data used in this study are openly accessible online, and cited and explained in the text. The forecast model data can be obtained by contacting author Dr. Shuqi Lin (shuqi.lin@queensu.ca). The Python code used for the COASTLINES were shown in the Appendices. The AEM3D can be installed and run with the licence purchased from Hydronumerics (http://www.hydronumerics.com.au/), and its source code is available with permission from Hydronumerics.

Author contributions.

The concept of the COASTLINES workflow was designed by LB, SL, SS, and RM, and SL carried them out. SL developed the model code and performed the simulations. All authors contributed to the validation of the model and interpretation of the results. SL wrote the manuscript with contributions from LB, SS, and RM.

Acknowledgements.

This project was funded by the Dean's Research Fund from the Faculty of Engineering and Applied Science at Queen's University. Computational support .was provided by Alexander Rey and FEAS-ITS. LB thanks Damien

https://doi.org/10.5194/gmd-2021-34
Preprint. Discussion started: 29 March 2021

Geoscientific Model Development
Discussions

Bouffard for discussions during visits to EAWAG, which inspired this research. James Homewood, from the Lower Thames Valley Conservation Authority (LTVCA) providing footages of the storm event on Nov. 15th, 2020.

Reference

Monthly water level bulletin: https://www.tides.gc.ca/C&A/bulletin-eng.html, last access: 5 Feb 2021.

Anderson, E. J., Fujisaki-Manome, A., Kessler, J., Lang, G. A., Chu, P. Y., Kelly, J. G. W., Chen, Y., and Wang, J.: Ice forecasting in the next-generation Great Lakes Operational Forecast System (GLOFS), J. Mar. Sci. Eng., 6, 10.3390/jmse6040123, 2018.

Antenucci, J., and Imerito, A.: The CWR dynamic reservoir simulation model DYRESM, Science Manual, The University of Western Australia, Perth, Australia, 2000.

Baracchini, T., Wüest, A., and Bouffard, D.: Meteolakes: An operational online three-dimensional forecasting platform for lake hydrodynamics, Water Res., 172, 10.1016/j.watres.2020.115529, 2020.

Beletsky, D., Hawley, N., Rao, Y. R., Vanderploeg, H. A., Beletsky, R., Schwab, D. J., and Ruberg, S. A.: Summer thermal structure and anticyclonic circulation of Lake Erie., Geophys. Res. Lett., 39, 10.1029/2012GL051002, 2012.

Bocaniov, S. A., and Scavia, D.: Temporal and spatial dynamics of large lake hypoxia: Integrating statistical and three-dimensional dynamic models to enhance lake management criteria, Water Resour. Res., 52, 4247-4263, 10.1002/2015WR018170, 2016.

Bocaniov, S. A., Lamb, K. G., Liu, W., Rao, Y. R., and Smith, R. E. H.: High sensitivity of lake hypoxia to air temperatures, winds, and nutrient loading: Insights from a 3-D lake model, Water Resour. Res., 56, 10.1029/2019WR027040, 2020.

Boegman, L., Loewen, M., Hamblin, P. F., and A., C. D.: Vertical mixing and weak stratification over zebra mussel colonies in western Lake Erie, Limnol. Oceanogr., 53, 1093-1110, 10.4319/lo.2008.53.3.1093, 2008.

Booij, N., Ris, R. C., and Holthuijsen, L. H.: A third-generation wave model for coastal regions 1. Model description and validation J. Geophys. Res. Oceans, 104, 7649–7666, 10.1029/98JC02622, 1999.

Bouffard, D., and Boegman, L.: Poincare´ wave–induced mixing in a large lake, Limnol. Oceanogr., 57, 1201-1216, 10.4319/lo.2012.57.4.1201, 2012.

Bouffard, D., and Lemmin, U.: Kelvin waves in Lake Geneva, J. Great Lakes Res., 39, 637-645, 10.1016/j.jglr.2013.09.005, 2013.

Bouffard, D., Boegman, L., Ackerman, J. D., Valipour, R., and Rao, Y. R.: Near-inertial wave driven dissolved oxygen transfer through the thermocline of a large lake, J. Great Lakes Res., 40, 300-307, 10.1016/j.jglr.2014.03.014, 2014.

Brookes, J. D., and Carey, C. C.: Resilence to blooms, Science, 334, 46-47, 10.1126/science.1207349, 2011.

Buehner, M., McTaggart-Cowan, R., Beaulne, A., Charette, C., Garand, L., Heilliette, S., Lapalme, E., Laroche, S., Macpherson, S. R., Morneau, J., and Zadra, A.: Implementation of deterministic weather forecasting systems based on ensemble–variational data assimilation at Environment Canada. Part I: the global system, Mon. Wea. Rev., 143, 2532-2559, 10.1175/MWR-D-14-00354.1, 2015.

Caramatti, I., Peeters, F., Hamilton, D., and Hofmann, H.: Modelling inter-annual and spatial variability of ice cover in a temperate lake with complex morphology, Hydrol. Process., 34, 691-704, 10.1002/hyp.13618, 2019.

Casulli, V., and Cheng, R.: Semi-implicit finite difference methods for three-dimensional shallow water flow. , Int. J. Numer. Methods Fluids 15, 629-648, 10.1002/fld.1650150602 1992.

https://doi.org/10.5194/gmd-2021-34
Preprint. Discussion started: 29 March 2021

Geoscientific Model Development
Discussions

Chen, Q., and Mynett, A. E.: Modelling algal blooms in the Dutch coastal waters by integrated numerical and fuzzy cellular automata approaches, Ecol. Mod., 199, 73-81, 10.1016/j.ecolmodel.2006.06.014, 2006.

Chen, C., Beardsley, R. C., Cowles, G., Qi, J., Lai, Z., Gao, G., Stuebe, D., Xu, Q., Xue, P., Ge, J., Ji, R., Tian, R., Huang, H., Wu, L., and Lin, H.: An unstructured grid, finite-volume community ocean model FVCOM user manual, SMAST/UMASSD Tech. Rep. 11-1101, 373 pp., Dartmouth, Mass., 2012.

Chu, P. Y., Kelley, J. G. W., Mott, G. V., Zhang, A., and Lang, G. A.: Development, implementation, and skill assessment of the NOAA/NOS Great Lakes Operational Forecast System, Ocean Dyn. , 61, 1305-1316, 10.1007/s10236-011-0424-5, 2011.

Gaudard, A., Schwefel, R., Vinnå, L. R., Schmid, M., Wüest, A., and Bouffard, D.: Optimizing the parameterization of deep mixing and internal seiches in one-dimensional hydrodynamic models: a case study with Simstrat v1.3, Geosci. Model Dev., 10, 3411-3423, 10.5194/gmd-10-3411-2017, 2017.

Gaudard, A., Vinnå, L. R., Bärenbold, F., Schmid, M., and Bouffard, D.: Toward an open-access of high-frequency lake modelling and statistics data for scientists and practitioners. The case of Swiss Lakes using Simstrat v2.1, Geosci. Model Dev., 12, 3955-3974, 10.5194/gmd-2018-336, 2019.

Gronewold, A. D., Anderson, E. J., and Smith, J.: Evaluating operational hydrodynamic models for real-time simulation of evaporation from large lakes, Geophys. Res. Lett., 46, 3263-3269, 10.1029/2019GL082289, 2019.

Gronewold, A. D., and Rood, R. B.: Recent water level changes across Earth's largest lake system and implications for future variability, J. Great Lakes Res., 45, 1-3, 10.1016/j.jglr.2018.10.012, 2019.

Hall, E.: Hydrodynamic Modelling of Lake Ontario, M.Sc. thesis, Department of Civil Engineering, Queen's University Canada, 135 pp., 2008.

Hamblin, P. F.: Great Lakes storm surge of April 6, 1979, J. Great Lakes Res., 5, 312-315, 10.1016/S0380-1330(79)72157-5, 1979.

Hamblin, P. F.: Meteorological forcing and water level fluctuations on Lake Erie, J. Great Lakes Res., 13, 436-453, 10.1016/S0380-1330(87)71665-7, 1987.

Hecky, R. E., Smith, R. E. H., Barton, D. R., Guildford, S. J., Taylor, W. D., Charlton, M. N., and Howell, T.: The nearshore phosphorus shunt: a consequence of ecosystem engineering by dreissenids in the Laurentian Great Lakes, Can. J. Fish. Aquat. Sci., 61, 1285-1293, 10.1139/F04-065, 2004.

Higgins, S. N., Hecky, R. E., and Guildford, S. J.: Environmental controls of cladophora growth dynamics in eastern Lake Erie: Application of the Cladophora Growth Model (CGM), J. Great Lakes Res., 32, 629-644, 10.3394/0380-1330(2006)32[629:ECOCGD]2.0.CO;2, 2006.

Hipsey, M. R., Bruce, L. C., and Hamilton, D. P.: GLM - General Lake Model. Model overview and user information, Technical Manual, The University of Western Australia, Perth, Australia., 2014.

Hodges, B. R., Imberger, J., Saggio, A., and Winters, K. B.: Modeling basin-scale internal waves in a stratified lake, Limnology and Oceanography, 45, 1603-1620, 10.4319/lo.2000.45.7.1603, 2000.

Hodges, B. R., and Dallimore, C.: Aquatic Ecosystem Model: AEM3D, v1. 0, User Manual, Hydronumerics, Australia, Melbourne, 2016.

León, L. F., Imberger, J., Smith, R. E. H., Hecky, R. E., Lam, D. C. L., and Schertzer, W. M.: Modeling as a tool for nutrient management in Lake Erie: a hydrodynamics study, J. Great Lakes Res., 31, 309-318, 10.1016/S0380-1330(05)70323-3, 2005.

León, L. F., Smith, R. E. H., Hipsey, M. R., Bocaniov, S. A., Higgins, S. N., Hecky, R. E., Antenucci, J. P., Imberger, J. A., and Guildford, S. J.: Application of a 3D hydrodynamic-biological model for seasonal and spatial dynamics of water quality and phytoplankton in Lake Erie, J. Great Lakes Res., 37, 41-53, 10.1016/j.jglr.2010.12.007, 2011.

Leonard, B. P.: The ULTIMATE conservative difference scheme applied to unsteady one-dimensional advection., Comp. Methods Appl. Mech. Eng., 88, 17-74, 1991.

Lesser, G. R., Roelvink, J. V., Van Kester, J. A. T. M., and Stelling, G. S.: Development and validation of a three-dimensional morphological model. , Coastal Engineering, 51, 883-915, 10.1016/j.coastaleng.2004.07.014, 2004.

Liu, W., Bocaniov, S. A., Lamb, K. G., and Smith, R. E. H.: Three dimensional modeling of the effects of changes in meteorological forcing on the thermal structure of Lake Erie, J. Great Lakes Res., 40, 827–840, 10.1016/j.jglr.2014.08.002, 2014.

Loewen, M., Ackerman, J. D., and Hamblin, P. F.: Environmental implications of stratification and turbulent mixing in a shallow lake basin, Can. J. Fish. Aquat. Sci. , 64, 43-57, 10.1139/F06-165, 2007.

Madani, M., Seth, R., León, L. F., Valipour, R., and McCrimmon, C.: Three dimensional modelling to assess contributions of major tributaries to fecal microbial pollution of lake St. Clair and Sandpoint Beach, J. Great Lakes Res., 46, 159-179, 10.1016/j.jglr.2019.12.005, 2020.

Meyer, T. P., and Dale, R. F.: Predicting daily insolation with hourly cloud heights and coverage, J. Climate Appl. Meteorol., 22, 537–545, 10.1175/1520-0450(1983)022<0537:PDIWHC>2.0.CO;2, 1983.

Michalak, A. a. M., Anderson, E. J., Beletsky, D., Boland, S., Bosch, N. S., Bridgeman, T. B., Chaffin, J. D., Cho, K., Confesor, R., Daloğlu, I., DePinto, J. V., Evans, M. A., Fahnenstiel, G. L., He, L., Ho, J. C., Jenkins, L., Johengen, T. H., Kuo, K. C., LaPorte, E., Liu, X., McWilliams, M. R., Moore, M. R., Posselt, D. J., Richards, R. P., Scavia, D., Steiner, A. L., Verhamme, E., Wright, D. M., and Zagorski, M. A.: Record-setting algal bloom in Lake Erie caused by agricultural and meteorological trends consistent with expected future conditions, Proceedings of the National Academy of Sciences, 110, 6448-6452, 10.1073/pnas.1216006110, 2013.

MOE: Lake Erie fish kill incident on September 1, 2012. Summary Report.Ontario Ministry of the Environment Southwestern Region 14 ((Available from OntarioMinistry of Environment).), 2012.

Nakhaei, N., Boegman, L., Mehdizadeh, M., and Loewen, M.: Hydrodynamic modeling of Edmonton storm-water ponds, Environ. Fluid Mech., 19, 305-327, 10.1007/s10652-018-9625-5, 2019.

O'Neil, J. M., Davis, T. W., Burford, M. A., and Gobler, C. J.: The rise of harmful cyanobacteria blooms: The potential roles of eutrophication and climate change, Harmful Algae, 14, 313-334, 10.1016/j.scitotenv.2011.02.001, 2012.

O'Reilly, C. M., Sharma, S., Gray, D. K., Hampton, S. E., Read, J. S., and Rowley, R. J., et al.: Rapid and highly variable warming of lake surface waters around the globe, Geophys. Res. Lett., 42, 10773-10781, 10.1002/2015GL066235., 2015.

Oveisy, A., Boegman, L., and Imberger, J.: Three-dimensional simulation of lake and ice dynamics during winter, limnol. Oceanogr., 57, 42-57, 10.4319/lo.2012.57.1.0043, 2012.

https://doi.org/10.5194/gmd-2021-34
Preprint. Discussion started: 29 March 2021

Geoscientific Model Development Discussions

Paturi, S., Boegman, L., and Rao, Y. R.: Hydrodynamics of eastern Lake Ontario and the upper St. Lawrence River, J. Great Lakes Res., 38, 194-204, 10.1016/j.jglr.2011.09.008, 2012.

Rao, Y. R., and Murthy, C. R.: Coastal boundary layer characteristics during summer stratification in Lake Ontario., J. Phys. Oceanogr., 31, 1088-1104, 10.1175/1520-0485(2001)031<1088:CBLCDS>2.0.CO;2, 2001.

Rao, Y. R., Hawley, N., Charlton, M. N., and Schertzer, W. M.: Physical processes and hypoxia in the central basin of Lake Erie, Limnol. Oceanogr., 53, 2007-2020, 10.4319/lo.2008.53.5.2007, 2008.

Rao, Y. R., Howell, T., Watson, S. B., and Abernethy, S.: On hypoxia and fish kills along the north shore of Lake Erie, J. Great Lakes Res., 40, 187-191, 10.1016/j.jglr.2013.11.007, 2014.

Rey, A., and Mulligan, R. P.: Influence of Hurricane Wind Field Variability on RealTime Forecast Simulations of the Coastal Environment, J. Geophys. Res. Oceans, 126, 10.1029/2020JC016489, 2021.

Rowe, M. D., Anderson, E. J., Beletsky, D., Stow, C. A., Moegling, S. D., and Chaffin, J. D., et al: Coastal upwelling influences hypoxia spatial patterns and nearshore dynamics in Lake Erie., J. Geophys. Res. Oceans, 124, 10.1029/2019JC015192, 2019.

Ruberg, S. A., Guasp, E., Hawley, N., Muzzi, R. W., Brandt, S. B., and Vanderploeg, H. A., et al.: Societal benefits of the Real-time Coastal Observation Network (ReCON): Implications for municipal drinking water quality., Mar. Technol. Soc. J., 42, 103-109, 10.4031/002533208786842471, 2008.

Saber, A., James, D. E., and Hannoun, I. A.: Effects of lake water level fluctuation due to drought and extreme winter precipitation on mixing and water quality of an alpine lake, Case Study: Lake Arrowhead, California, Sci. Total Environ., 714, 10.1016/j.scitotenv.2020.136762, 2020.

Scavia, D., Allan, J. D., Arend, K. K., Bartell, S., Beletsky, D., Bosch, N. S., Brandt, S. B., Briland, R. D., Daloglu, I., DePinto, J. V., Dolan, D. M., and Evans, M. A. e. a.: Assessing and addressing the re-eutrophication of Lake Erie: Centralbasin hypoxia, J. Great Lakes Res., 40, 226-246, 10.1016/j.jglr.2014.02.004, 2014.

Scavia, D., DePinto, J. V., and Bertani, I.: A multi-model approach to evaluating target phosphorus loads for Lake Erie, J. Great Lakes Res., 42, 1139-1150, 10.1016/j.jglr.2016.09.007, 2016.

Schwab, D. J., and Beletsky, D.: Propagation of kelvin waves along irregular coastlines in finite-difference models., Adv. Water Resour., 22, 239-245, 10.1016/S0309-1708(98)00015-3, 1998.

Schwab, D. J., Leshkevich, G. A., and Muhr, G. C.: Automated Mapping of Surface Water Temperature in the Great Lakes, J. Great Lakes Res., 25, 468-481, 10.1016/S0380-1330(99)70755-0, 1999.

Hundreds of dead fish wash up in Sandusky Bay: https://www.13abc.com/content/news/Hundreds-of-dead-fish-wash-up-in-Sandusky-Bay-571025541.html, last access: 5 February 2021.

Trebitz, A. S.: Characterizing seiche and tide-driven daily water level fluctuations affecting coastal ecosystems of the Great Lakes, J. Great Lakes Res., 32, 102-116, 10.3394/0380-1330(2006)32[102:CSATDW]2.0.CO;2, 2006.

Valipour, R., Bouffard, D., Boegman, L., and Rao, Y. R.: Near-inertial waves in Lake Erie, Limnol. Oceanogr., 60, 1522–1535, 10.1021/es301422r, 2015.

Valipour, R., Rao, Y. R., León, L. F., and Depew, D.: Nearshore-offshore exchanges in multi-basin coastal waters: Observations and three-dimensional modeling in Lake Erie, J. Great Lakes Res., 45, 50-60, 10.1016/j.jglr.2018.10.005, 2019.

https://doi.org/10.5194/gmd-2021-34
Preprint. Discussion started: 29 March 2021

Geoscientific Model Development
Discussions

Watson, S. B., Miller, C., Arhonditsis, G., Boyer, G. L., and al, e.: The re-eutrophication of Lake Erie: Harmful algal blooms and hypoxia, Harmful Algae, 56, 44-66, 10.1016/j.hal.2016.04.010, 2016.

Woolway, R. I., and Merchant, C. J.: Worldwide alteration of lake mixing regimes in response to climate change., Nat. Geosci., 12, 271-276, 10.1038/s41561-019-0322-x, 2019.

Woolway, R. I., Kraemer, B. M., and Lenters, J. D., et al.: Global lake responses to climate change, Nat Rev Earth Environ, 10.1038/s43017-020-0067-5, 2020.

https://doi.org/10.5194/gmd-2021-34
Preprint. Discussion started: 29 March 2021

Appendix A: Code for retrieving observational data

A1: Water level from gauges

```
from selenium import webdriver
import urllib
import os
import requests
import csv
from datetime import datetime
from bs4 import BeautifulSoup
import time
import matlab.engine
import calendar

dt = datetime.now()
last_day_of_month = calendar.monthrange(dt.year, dt.month)[1]
name_month = calendar.month_name[dt.month][:3]
Mon = str(dt.month)+'%2F'+str(last_day_of_month)

name_Bar_point = 'Bar Point_waterlevel_'+name_month+'.csv'
name_Kingsville = 'Kingsville_waterlevel_'+name_month+'.csv'
name_Erieau = 'Erieau_waterlevel_'+name_month+'.csv'
name_Colborne = 'Colborne_waterlevel_'+name_month+'.csv'
name_Dover = 'Dover_waterlevel_'+name_month+'.csv'
name_Stanley = 'Stanley_waterlevel_'+name_month+'.csv'

os.chdir('…\observation\water level')
try:
    os.remove(name_Bar_point)
    os.remove(name_Kingsville)
    os.remove(name_Erieau)
    os.remove(name_Colborne)
    os.remove(name_Dover)
    os.remove(name_Stanley)
except:
    os.chdir('…\observation\water level')

Barpoint_page
='https://marees.gc.ca/eng/Station/Month?type=1&sid=12005&tz=EST&pres=2&date=2020%2F'+ Mon
Kingsville_page =
'https://marees.gc.ca/eng/Station/Month?type=1&sid=12065&tz=EST&pres=2&date=2020%2F'+ Mon
Erieau_page =
'https://marees.gc.ca/eng/Station/Month?type=1&sid=12250&tz=EST&pres=2&date=2020%2F'+ Mon
Colborne_page =
'https://marees.gc.ca/eng/Station/Month?type=1&sid=12865&tz=EST&pres=2&date=2020%2F'+ Mon
Dover_page =
'https://marees.gc.ca/eng/Station/Month?type=1&sid=12710&tz=EST&pres=2&date=2020%2F'+ Mon
Stanley_page =
'https://marees.gc.ca/eng/Station/Month?type=1&sid=12400&tz=EST&pres=2&date=2020%2F'+ Mon

def retrieve_from_web(stationpage,stationname):
    page = requests.get(stationpage)
    page.raise_for_status()
    soup = BeautifulSoup(page.text)
    data = soup.find("div",class_="stationTextData")
```

https://doi.org/10.5194/gmd-2021-34
Preprint. Discussion started: 29 March 2021


```
        with open(stationname, 'a') as csv_file:
            writer = csv.writer(csv_file,lineterminator ='\n')
            writer.writerow(['Date','Time','WL'])

        for i in range(1,len(data.contents),2):
            each_data = str(data.contents[i])
            each_data = each_data.split()[1].split(";")
            Date = each_data[0]
            Time = each_data[1]
            WL = each_data[2]
            with open(stationname, 'a') as csv_file:
                writer = csv.writer(csv_file,lineterminator ='\n')
                writer.writerow([Date,Time,WL])

    retrieve_from_web(Barpoint_page,name_Bar_point)
    retrieve_from_web(Kingsville_page,name_Kingsville)
    retrieve_from_web(Erieau_page,name_Erieau)
    retrieve_from_web(Colborne_page,name_Colborne)
    retrieve_from_web(Dover_page,name_Dover)
    retrieve_from_web(Stanley_page,name_Stanley)
```

https://doi.org/10.5194/gmd-2021-34
Preprint. Discussion started: 29 March 2021

Geoscientific Model Development
Discussions
Open Access

A2: Lake buoy data acquisition examples

```
from selenium import webdriver
import urllib
import os
import requests
import csv
from datetime import datetime
from bs4 import BeautifulSoup
import time

Month = datetime.now().month
Date = datetime.now().day

def data_NDBC(station_web,station_name):
    page  = requests.get(station_web)
    page.raise_for_status()
    soup = BeautifulSoup(page.text)
    each_line = soup.contents[0].split('\n')
    for i in range(0,2):
        each_data = each_line[i]
        with open(station_name , 'a') as csv_file:
            writer = csv.writer(csv_file,lineterminator = '\r')
            writer.writerow([each_data])
    for i in range(len(each_line)-2,2,-1):
        each_data = each_line[i]
        with open(station_name , 'a') as csv_file:
            writer = csv.writer(csv_file,lineterminator = '\n')
            writer.writerow([each_data])

## Station 45142 from NDBC
name_45142 = "STN 45142_" + str(Month) + "." + str(Date)+".csv"
os.chdir('…\\observation\\temperature\\STN45142')
try:
    os.remove(name_45142)
except:
    os.chdir('…\\observation\\temperature\\STN45142')
website1 = 'https://www.ndbc.noaa.gov/data/realtime2/45142.txt'
data_NDBC(website1,name_45142)

## Station 45167 from GLOS
def retrieve_45167():
    for name_45167 in glob.glob('.../Downloads/*45167*'):
        print name_45167
    try:
        os.remove(name_45167)
    except:
        os.chdir('…/14sl105/Downloads')
    driver = webdriver.Chrome()
    driver.get("https://glbuoys.glos.us/tools/export?data_type=buoy&units=eng&locs=45167")
    select_bottom = list()
    select_bottom.append("//*[@id='btn-clearParam']")
    select_bottom.append("//*[@id='Wind_Speed']")
    select_bottom.append("//*[@id='Wind_from_Direction']")
    select_bottom.append("//*[@id='Water_Temperature_at_Surface']")
    select_bottom.append("//*[@id='Air_Temperature']")
```

https://doi.org/10.5194/gmd-2021-34
Preprint. Discussion started: 29 March 2021

Geoscientific Model Development
Discussions
Open Access

```
    try:
        for i in select_bottom:
            elem = driver.find_elements_by_xpath(i)
            elem[0].click()
    except:
        for i in range(0,len(select_bottom)):
            elem = driver.find_elements_by_xpath(select_bottom[i])
            elem[0].click()

    download_bottom = "//*[@id='btn-download']"
    elem2 = driver.find_elements_by_xpath(download_bottom)
    elem2[0].click()

    time.sleep(3)
    driver.quit()
    for name_45167 in glob.glob('…/Downloads/*45167*'):
        print name_45167

    f45167 = pd.read_excel(name_45167,header = 5)
    Time = f45167[['Date/Time (UTC)']]
    air_temp = (f45167[['Air_Temperature (fahrenheit)']]-32)*5/9
    surf_temp = (f45167[['Water_Temperature_at_Surface (fahrenheit)']]-32)*5/9
    wind_spd = (f45167[['Wind_Speed (kts)']])/1.944
    wind_dir = f45167[['Wind_from_Direction (degrees_true)']]
    select_column = pd.concat([Time,surf_temp,air_temp,wind_spd,wind_dir],axis= 1)
    select_column.columns = ['Time in UTC','Surf_temp (C)','air temp(C)','wind speed (m/s)','wind direction']
    select_column.to_csv(r'…\observation\temperature\STN45167\temp '+str(Month) + "." +
str(Date)+'.csv',index = None, header = True)
try:
    retrieve_45167()
except:
    print('Can not retrieve observations from buoy 45167')
```

https://doi.org/10.5194/gmd-2021-34
Preprint. Discussion started: 29 March 2021

A3: Lake surface temperature from satellite imagery

```
from selenium import webdriver
import urllib
import os
import requests
from datetime import datetime
from bs4 import BeautifulSoup
import time

YY = datetime.now().year
MM = datetime.now().month
DD = datetime.now().day
if DD<3:
    MM = MM-1
if MM<10:
    MM = "0" + str(MM)
else:
    MM = str(MM)

page = "https://coastwatch.glerl.noaa.gov/erddap/files/GLSEA_GCS/" + str(YY) + "/" + MM + "/"
print(page)
driver = webdriver.Chrome()
driver.get(page)

def retrieve_satellite():
    html = urllib.urlopen(page).read()
    soup = BeautifulSoup(html, 'html.parser')
    tags = soup('a')
    nclst = list()
    for tag in tags:
        if tag.get('href').endswith('.nc'):
            print(str(tag.get('href')))
            nclst.append(str(tag.get('href')))

    url = page + nclst[-1]
    res = requests.get(url, allow_redirects=True)
    print(res.raise_for_status())
    os.chdir("…\observation\satellite data")
    open(nclst[-1], 'wb').write(res.content)

    time.sleep(3)
    driver.quit()

try:
    retrieve_satellite()
except:
    print('No data today')
    driver.quit()
```

https://doi.org/10.5194/gmd-2021-34
Preprint. Discussion started: 29 March 2021

Appendix B: COASTLINE website snapshot

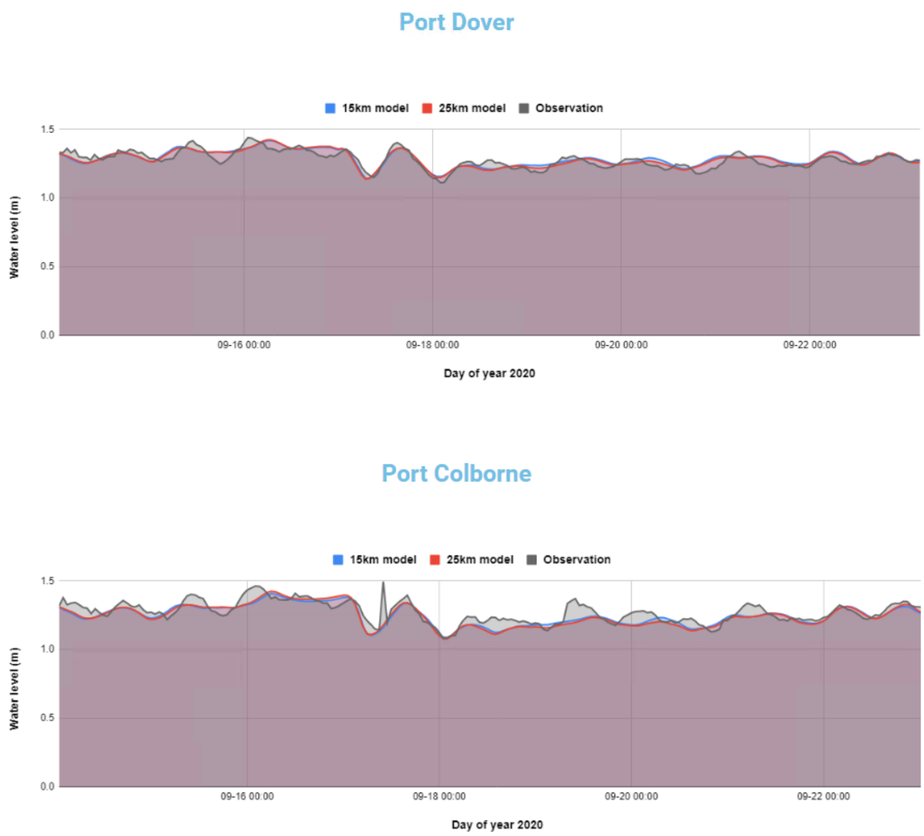

Fig. B1 Snapshot of water level forecast validation web page displayed on COASTLINES online platform: https://coastlines.engineering.queensu.ca/erie/water-level-forecast/. Status on Sep 23rd, 2020.

https://doi.org/10.5194/gmd-2021-34
Preprint. Discussion started: 29 March 2021

Geoscientific Model Development Discussions

Appendix C: Validation of meteorological input variables

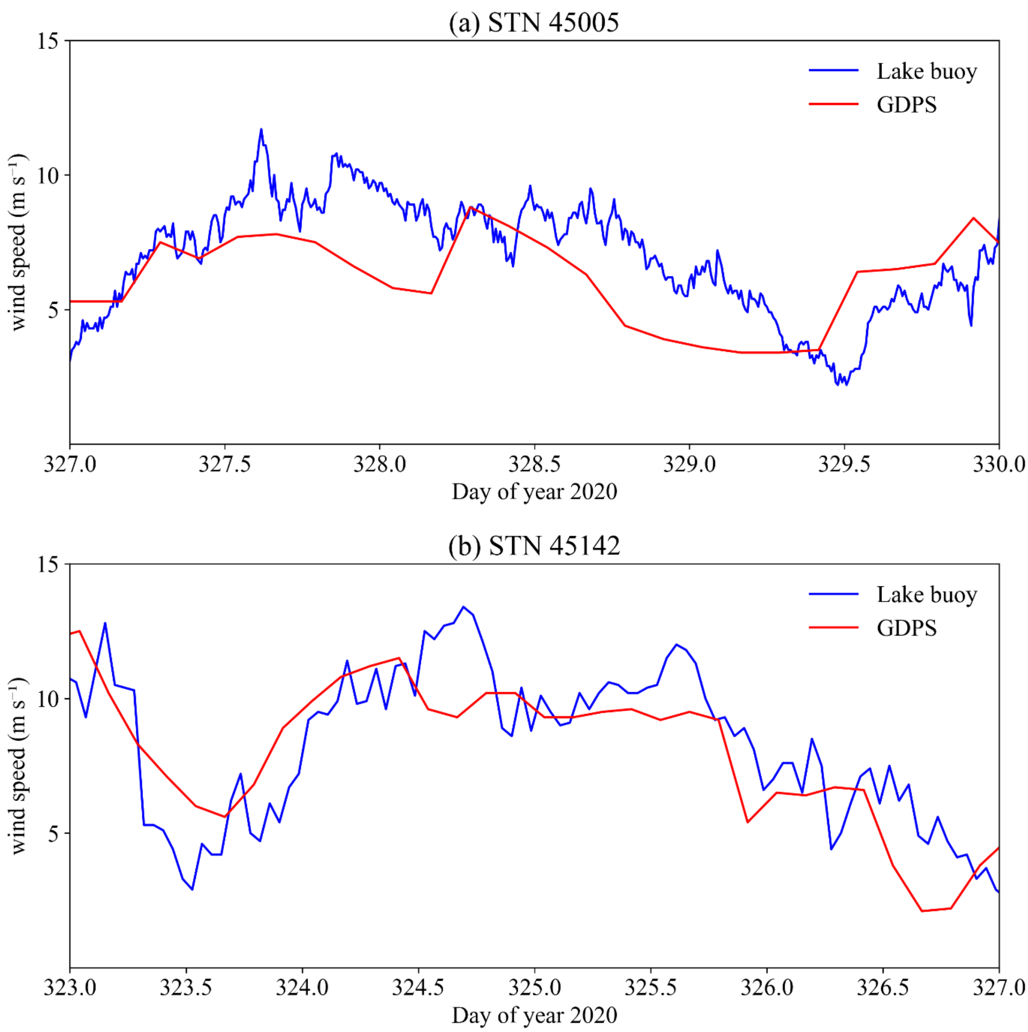

Fig. C1 Comparisons of stitched GDPS wind forecast with 3 h delivery interval and lake buoy measured wind speed at (a) station 45005 (10 min sampling interval), and (b) station 45142 (1 h sampling interval). The wind gusts on day 327 at station 45005 and day 324 at station 45142 were missed by wind forecast.

https://doi.org/10.5194/gmd-2021-34
Preprint. Discussion started: 29 March 2021

Geoscientific Model Development Discussions

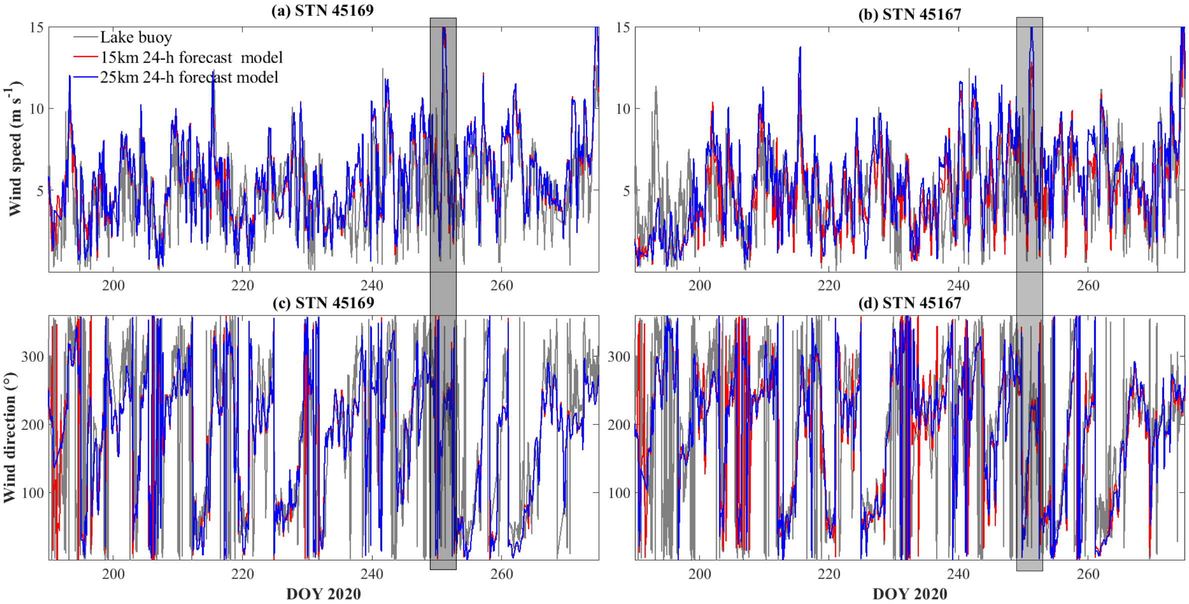

8

835 **Fig. C2 Comparisons of 24-h meteorological forecast and lake buoy observations of wind speed (a, b) and wind**
836 **direction (c, d). The gray rectangle indicates the storm that led to up-welling along northern shoreline on days**
837 **248-253.**

https://doi.org/10.5194/gmd-2021-34
Preprint. Discussion started: 29 March 2021

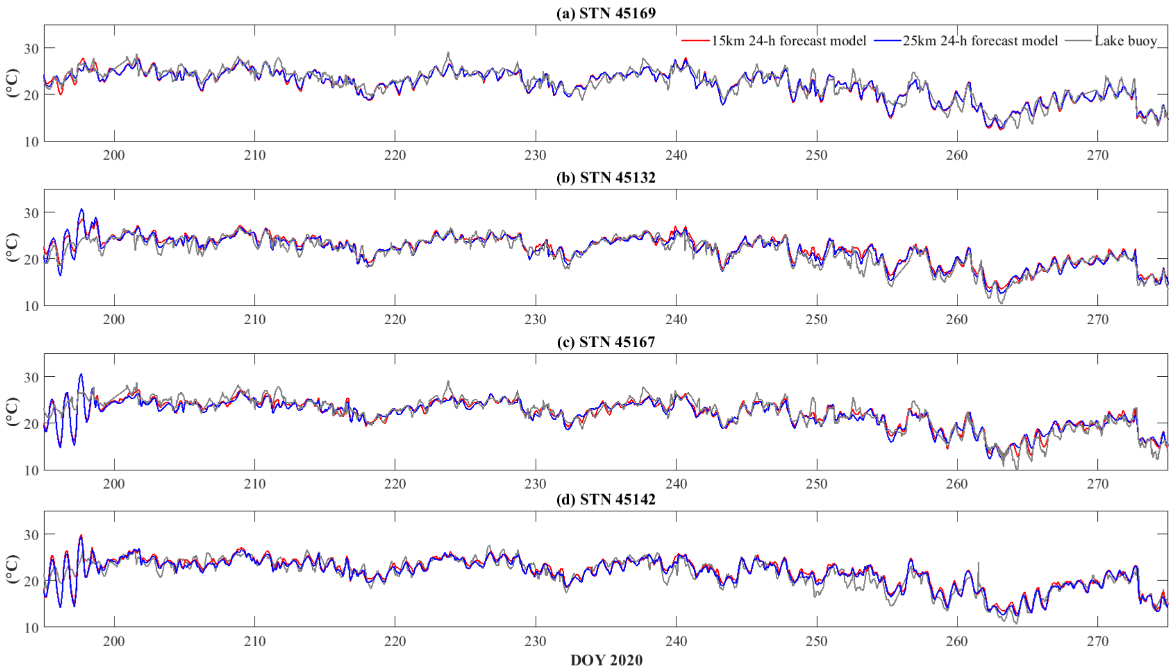

Fig. C3 Comparisons of 24-h air temperature forecast and lake buoy observations of air temperature.

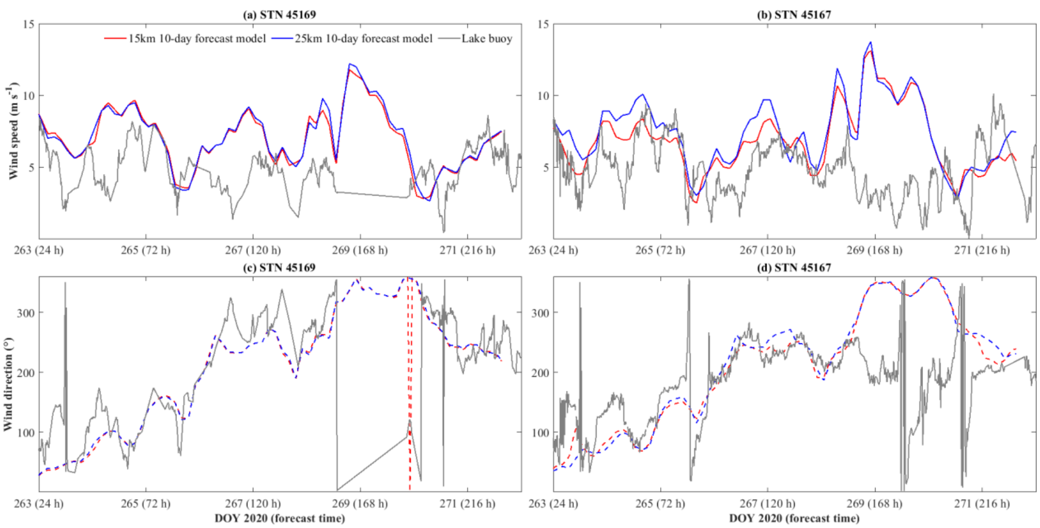

Fig. C4 Comparisons of 240-h meteorological forecast and lake buoy observations of wind speed (a, b) and wind direction (c, d).

https://doi.org/10.5194/gmd-2021-34
Preprint. Discussion started: 29 March 2021

Geoscientific Model Development Discussions

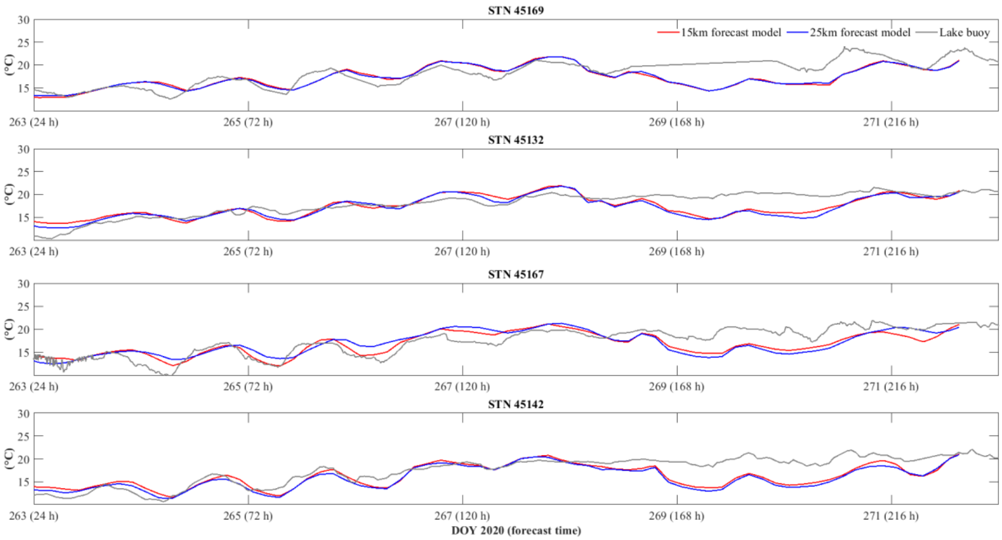

844

845 **Fig. C5 Comparisons of 240-h air temperature forecast and lake buoy observations.**

https://doi.org/10.5194/gmd-2021-34
Preprint. Discussion started: 29 March 2021

Geoscientific Model Development
Discussions

Appendix D: Temperature validation against satellite observations

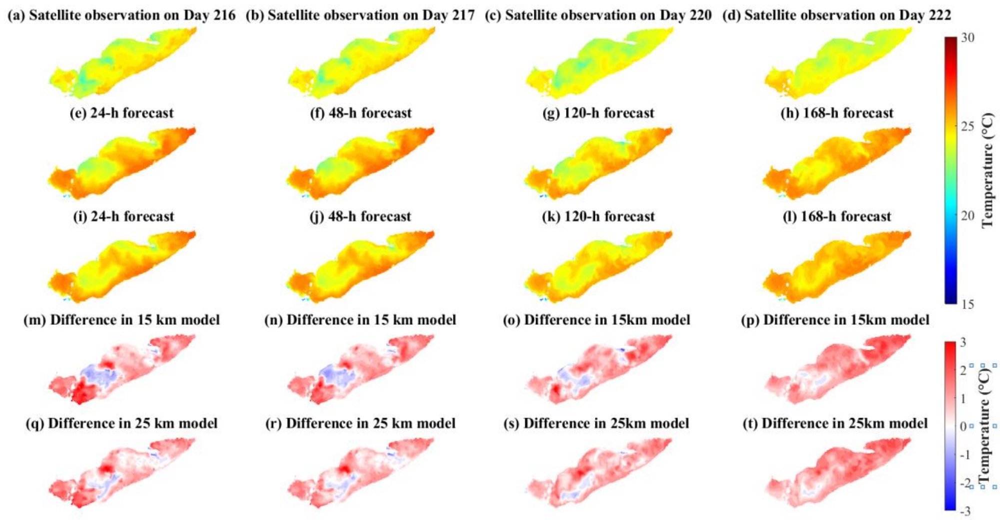

Fig. D1 comparisons of (a-d) satellite observations, (e-h) 15 km model forecast, and (i-l) 25 km model forecast during summer. The difference between observations and models are shown in (m-t).

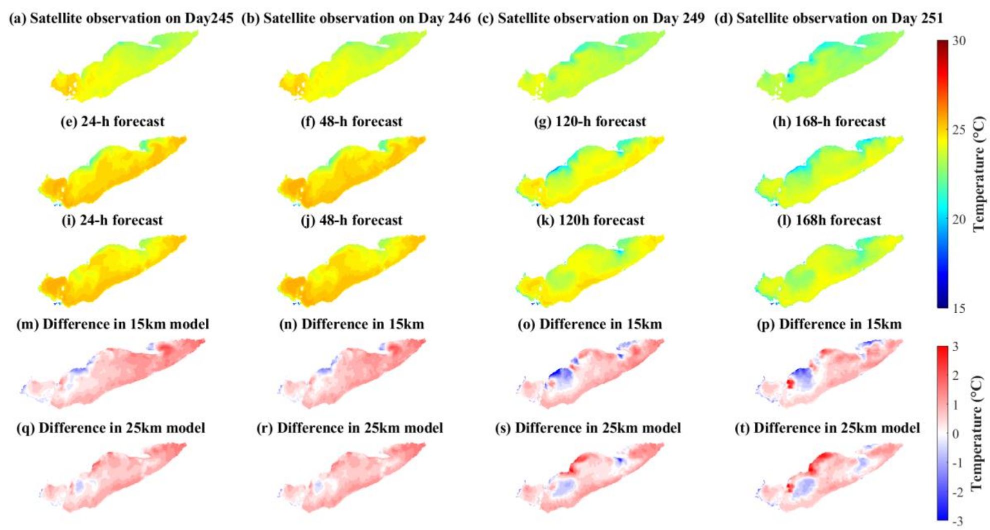

Fig. D2 comparisons of (a-d) satellite observations, (e-h) 15 km model forecast, and (i-l) 25 km model forecast during late summer. The difference between observations and models are shown in (m-t).